Journal of Applied Analysis and Computation
Volume 15, Number 3, June 2025, 1241–1271
Website:http://www.jaac-online.com
DOI:10.11948/20240181

BIFURCATION AND CHAOS IN A DISCRETE FRACTIONAL ORDER REDUCED LORENZ MODEL WITH CAPUTO AND CONFORMABLE DERIVATIVES

S. M. Sohel Rana[1], Md. Jasim Uddin[1,†] and A. Q. Khan[2]

Abstract This study investigates a discrete fractional order reduced Lorenz model that incorporates the Caputo and Conformable fractional derivatives respectively. The stability of equilibrium points of the model with Caputo fractional derivative are analyzed. The Conformable fractional derivative model is likewise examined. We confirm algebraically the existence and direction of Neimark-Sacker bifurcation for both models using the central manifold and bifurcation theories. The dynamic behavior of these models have been extensively investigated based on changes made to the control parameters. In addition to supporting analytical findings, numerical simulations are used to reveal chaotic characteristics such as bifurcations, phase portraits, periodic orbits, invariant closed cycles, and attractive chaotic sets. We also quantitatively compute the maximal Lyapunov exponents and fractal dimensions to validate the chaotic properties of the system. Using three different control strategies viz, OGY, hybrid control method, and state feedback method, the system's chaotic trajectory is finally stopped.

Keywords Reduced Lorenz model, Caputo and Conformable fractional derivatives, bifurcations, chaos control.

MSC(2010) 37C25, 37D45, 40A05, 39A33, 70K50.

1. Introduction

The numerous definitions of real number powers or complex number powers of the differentiation operator had been explored using the area of mathematical analysis known as fractional calculus. Fractional calculus was first introduced in the 17th century. Nevertheless, it might be regarded as a novel study topic. Fractional-order differential equations are an excellent tool for characterizing memory and hereditary properties of many systems [47] since the fractional derivative operator is non-local. Compared to equivalents in integer-order differential equations (IDEs), findings can be more precise [13, 15, 34]. Numerous fields can be effectively explained using Fractional-order differential equations, as stated in [28–31, 53]. When transitioning

†The corresponding author.
[1]Department of Mathematics, University of Dhaka, Dhaka 1000, Bangladesh
[2]Department of Mathematics, University of Azad Jammu and Kashmir, Muzaffarabad 13100, Pakistan
Email: srana.mthdu@gmail.com(S. M. Sohel Rana),
jasimu00@gmail.com(Md. Jasim Uddin),
abdulqadeerkhan1@gmail.com(A. Q. Khan)

from IDEs to Fractional-order differential equations, precision is necessary about the order of derivatives; even a small variations in order α_d might significantly impact the result [10]. Fractional differential equations are useful in explaining situations that IDEs are not able to fully replicate [32]. Similar to a nonlinear differential system, a nonlinear fractional differential system displays the intricate dynamics of chaos and bifurcation. Investigating the chaotic behavior of fractional-order differential systems is an intriguing and captivating field of study [2,5,11,12,21,58]. There are several approaches to deal with arbitrary order using the concept of differentiation. The definitions that are most frequently used are Riemann-Liouville, Caputo, and Grünwald-Letnikov [48]. By using these definitions, researchers make sure to always use the best method when developing or adjusting their models, including specific numerical techniques [8, 33, 43]. Fractional-order Lorenz systems have been studied by many scholars [18, 26, 41, 57, 59, 63]. Furthermore, discrete fractional-order systems have also been examined [44, 62] and found to exhibit rich dynamic properties based on the concept of fractional difference.

In a continuous dynamical system, Lorenz [40] presented his search for a three-dimensional set of ordinary differential equations that could simulate some of the unexpected behavior that we typically associate with the weather. The model is given by

$$\begin{aligned} x'(t) &= a_1(y-x), \\ y'(t) &= c_1 x - y - xz, \\ z'(t) &= xy - b_1 z. \end{aligned} \tag{1.1}$$

In system (1.1) $x, y, z \in \mathbb{R}$ are the state variables denoting the rate of convective overtuning, horizontal temperature difference, and vertical temperature difference, respectively. The parameters $a, b_1, c_1 \in \mathbb{R}^+$ in the system represent the Prandal number, the Rayleigh number, and some physical proportions of the region under study. For more description of these parameters, we refer [55]. The chosen limiting form of system (1.1) as $a_1 \to \infty$ while b_1 and c_1 remain fixed, and letting $a = (c_1 - 1), b_1 = 1$ and denoting the dependent variables by x and y instead of y and z, the reduced Lorenz (1989) system [40] is given by

$$\begin{aligned} x'(t) &= ax - xy, \\ y'(t) &= -y + x^2. \end{aligned} \tag{1.2}$$

The numerical analysis of the system (1.2) was provided in [24, 40], which marks a turning point in the investigation of the notion of computational chaos. It has been demonstrated that it (discrete case) possesses a more extensive collection of dynamical patterns than those noticed in the continuous case. However, while many academics have thoroughly examined systems bifurcation in continuous dynamical systems, only a small number of studies have focused on systems bifurcation in discrete dynamical systems. Many two-dimensional discrete systems, such as those involving stable orbits, chaotic attractors, Neimark-Sacker, and period-doubling bifurcations, are of interest to researchers (see [22, 35, 38, 39, 45, 50–52, 54]). It is possible to scientifically quantify these behaviors. Gao and Liu [25] also investigated the dynamical characteristics of a discrete two-dimensional system. Hu et al. [27] investigated the stability and bifurcations of a discrete predator-prey model with a nonmonotonic functional response. The behavior of a discrete-time model that describes the interaction between prey and predator, including the impact of

harvesting on the predator, is thoroughly examined in [23]. In [7], an in-depth investigation is conducted into the local stability of the fixed points and the Neimark-Sacker bifurcation at the positive fixed point. The study in [56], analyzes a discrete Leslie—Gower predator—prey model incorporating herd behavior, with a particular focus on how the slow–fast effect impacts predator dynamics. R. Ahmed et al. in [6] explores a slow–fast discrete predator-–prey interaction model that includes prey refuge and herd behavior to uncover its complex dynamics. The strong resonance bifurcation of a discrete-time Bazykin—Berezovskaya prey-predator model with a strong Allee effect is rigorously investigated in [46]. Agiza et al. [4] showed that the discrete system exhibits considerably richer dynamics than the continuous one when examining the chaotic dynamics of a discrete prey-predator model with Holling Type II response. The use of chaotic dynamics in information security is a recent development in encryption research. It has been shown that encryption-based chaotic maps perform better than other approaches, and that chaotic maps share many significant properties with the underlying assumptions of traditional encryption algorithms [61]. For instance, ergodicity, aperiodicity, sensitive dependency on initial conditions, and random-like behaviors. So, encryption may take advantage of a discrete reduced Lorenz system. On the other hand, in 2014, Elabbasy et al. [20] examined the bifurcations and chaos in a following discrete reduced Lorenz system:

$$\begin{aligned} x_{n+1} &= (1+ah)x_n - hx_n y_n, \\ y_{n+1} &= (1-h)x_n + hx_n^2. \end{aligned} \tag{1.3}$$

Which is a discrete version of the continuous-time system, which is depicted in (1.2), be Euler-forward formula where h is the integral step size. More precisely, Elabbasy et al. [20] studied the existence and local stability at fixed points of the system (1.3). Furthermore, by the center manifold theorem and bifurcation theory, authors derive the conditions for the existence of a flip bifurcation, pitchfork bifurcation and Neimark—Sacker bifurcation. Finally, authors verified the theoretical results numerically. As compared to the work of Elabbasy et al. [20], in the presented work, we first derived the discrete system by Caputo and Conformable fractional derivatives, and then stability, bifurcation, and chaos control are given. Finally, theoretical results are numerically confirmed.

In the current study, we employ the Caputo and Conformable fractional derivatives to the continuous system (1.2) and provide a theoretical explanation of the bifurcation events. Currently, a small number of authors [1–3,5,11,12,14,21,49] use Caputo fractional derivative in discrete models. Fractional derivatives are defined in many ways. One of the most popular definitions of fractional derivatives is the one given forth by Caputo 1.1, and it is widely employed in real-world applications.

Definition 1.1. Consider

$$D^{\alpha_d} f(t) = J^{l-\alpha_d} f^{(l)}(t), \quad \alpha_d > 0$$

where f^l represents the derivative of $f(t)$ of order l, also

$$J^q h(t) = \frac{\int_0^t (t-\tau_e)^{q-1} h(\tau_e) d\tau_e}{\Gamma(q)}, \quad q > 0.$$

The fractional order form for the model (1.2) is as follows,

$$\begin{aligned} D^{\alpha_d} x(t) &= ax(t) - x(t)y(t), \\ D^{\alpha_d} y(t) &= -by(t) + x^2(t). \end{aligned} \tag{1.4}$$

Apart from the definition of Caputo fractional derivative, Khalil et al. [37] proposed a new term named "Conformable fractional derivative". This definition states that the function's left fractional derivative begins at a, $f : [a, \infty) \to \infty$ of order $0 < \alpha_d < 1$ has the following limit-based definition 1.2:

Definition 1.2. Let

$$\left(T^a_{\alpha_d} f\right)(t) = \lim_{\tilde{\epsilon} \to 0} \frac{f\left(t + \tilde{\epsilon}(t-a)^{1-\alpha_d}\right) - f(t)}{\tilde{\epsilon}},$$

provided the limit exists. Following is the definition of the right fractional derivative of order $0 < \alpha_d < 1$ terminating at b of f.

$$\left({}^b_{\alpha_d} T f\right)(t) = -\lim_{\tilde{\epsilon} \to 0} \frac{f\left(t + \tilde{\epsilon}(b-t)^{1-\alpha_d}\right) - f(t)}{\tilde{\epsilon}}.$$

Also, take note that the following equality exists if f is differentiable in the normal sense:

$$\left(T^a_{\alpha_d} f\right)(t) = (t-a)^{1-\alpha_d} f'(t), \quad \left({}^b_{\alpha_d} T f\right)(t) = (t-b)^{1-\alpha_d} f'(t).$$

Following is provided for the model(1.2)'s Conformable fractional order version

$$\begin{aligned} T_{\alpha_d} x(t) &= ax(t) - x(t)y(t), \\ T_{\alpha_d} y(t) &= -by(t) + x^2(t). \end{aligned} \tag{1.5}$$

The aforementioned definition has been developed to remove challenges brought on by Caputo fractional derivative in applications [9]. It shares certain characteristics with the ordinary derivative. The conformable fractional derivative is a logical extension of the classical derivative, even if it might not be a fractional derivative in the sense of Caputo and it has a fractional order. Applications of the conformable derivative in biology and physics were studied in [9, 12, 17, 36]. It is true that Conformable fractional derivatives enable the inclusion of memory effects in the model. Like other types of fractional derivatives, conformable fractional derivatives consider not only the current state of a system but also its past states, allowing the model to incorporate memory effects. This makes them useful for accurately representing systems where historical behavior influences current dynamics.

The key findings explained in this article can be summed up as follows:
(1) We introduce a new discrete-time Lorenz model based on conformable fractional derivatives and Caputo derivatives. The distinct features of some meteorological occurrences can be captured by this model.
(2) The existence and stability of the equilibrium points were thoroughly examined in the first stage.
(3) We investigate the bifurcation behavior of both systems (specifically, the Neimark-Sacker bifurcation) using the center manifold theorem and normal form theory.
(4) We examine a method known as the $0-1$ chaos test for analyzing the chaotic characteristics of a discrete dynamical system.
(5) The research concludes by examining how well state feedback, hybrid control techniques, and Ott-Grebogi-Yorke (OGY) work to manage chaotic trajectory inside the system.
(6) Lastly, the accuracy and effectiveness of our theoretical and mathematical ideas are assessed using the numerical simulation section.

This study aims to compare the acquired results and explore the dynamic behavior of the discretized conformable fractional order model and the discretized caputo fractional order model. It follows the structure shown below. In Sections 2 and 3 treat the discretization process based on piecewise constant arguments applied to the model's conformable fractional-order form and caputo, yielding a two-dimensional discrete dynamical system. Furthermore, we examine the stability and bifurcation analysis of the discrete model. Section 4 presents numerical results incorporating bifurcation diagrams, phase portraits, MLEs, and FDs. We use OGY, state feedback and hybrid control strategy in Section 5 to eliminate the chaos of the uncontrolled system. A brief discussion is presented in Section 6.

2. Reduced Lorenz system with Caputo fractional derivative

2.1. Discretization

To discretize system (1.4), we use the piecewise constant approximation (PCA) [3,36,49]. The steps are as follows:

Assume that the initial conditions of system (1.4) are $x(0) = x_0, y(0) = y_0$. We write the system (1.4) as:

$$\begin{aligned} D^{\alpha_d}x(t) &= ax([\frac{t}{\rho_d}]) + x([\frac{t}{\rho_d}]\rho_d)y([\frac{t}{\rho_d}]\rho_d), \\ D^{\alpha_d}y(t) &= -by([\frac{t}{\rho_d}]\rho_d) + x^2([\frac{t}{\rho_d}]\rho_d). \end{aligned}$$

First, let $t \in [0, \rho_d)$, so $\frac{t}{\rho_d} \in [0, 1)$. Thus, we obtain

$$\begin{aligned} D^{\alpha_d}x(t) &= ax_0 - x_0y_0, \\ D^{\alpha_d}y(t) &= -by_0 + x_0^2. \end{aligned} \tag{2.1}$$

The solution of (2.1) is reduced to

$$\begin{aligned} x_1(t) &= x_0 + J^{\alpha_d}\left(ax_0 - x_0y_0\right) = x_0 + \frac{t^{\alpha_d}}{\alpha_d\Gamma(\alpha_d)}\left(ax_0 - x_0y_0\right), \\ y_1(t) &= y_0 + J^{\alpha_d}\left(-by_0 + x_0^2\right) = y_0 + \frac{t^{\alpha_d}}{\alpha_d\Gamma(\alpha_d)}\left(-by_0 + x_0^2\right). \end{aligned}$$

Next, let $t \in [\rho_d, 2\rho_d)$, so $\frac{t}{\rho_d} \in [1, 2)$. Then

$$\begin{aligned} D^{\alpha_d}x(t) &= ax_1 - x_1y_1, \\ D^{\alpha_d}y(t) &= -by_1 + x_1^2, \end{aligned}$$

and the solution becomes

$$\begin{aligned} x_2(t) &= x_1(\rho_d) + J_{\rho_d}^{\alpha_d}\left(ax_1 - x_1y_1\right) \\ &= x_1(\rho_d) + \frac{(t-\rho_d)^{\alpha_d}}{\alpha_d\Gamma(\alpha_d)}\left(ax_1 - x_1y_1\right), \\ y_2(t) &= y_1(\rho_d) + J_{\rho_d}^{\alpha_d}\left(-by_1 + x_1^2\right) \\ &= y_1(\rho_d) + \frac{(t-\rho_d)^{\alpha_d}}{\alpha_d\Gamma(\alpha_d)}\left(-by_1 + x_1^2\right), \end{aligned}$$

where $J_{\rho_d}^{\alpha_d} \equiv \frac{1}{\Gamma(\alpha_d)} \int_{\rho_d}^{t} (t-\tau_e)^{\alpha_d - 1} d\tau_e, \quad \alpha_d > 0$. After n times repetition, we obtain

$$\begin{aligned} x_{n+1}(t) &= x_n(n\rho_d) + \frac{(t-n\rho_d)^{\alpha_d}}{\alpha_d \Gamma(\alpha_d)} \left(a x_n(n\rho_d) - x_n(n\rho_d) y_n(n\rho_d)\right), \\ y_{n+1}(t) &= y_n(n\rho_d) + \frac{(t-n\rho_d)^{\alpha_d}}{\alpha_d \Gamma(\alpha_d)} \left(-b y_n(n\rho_d) + x_n^2(n\rho_d)\right), \end{aligned} \tag{2.2}$$

where $t \in [n\rho_d, (n+1)\rho_d)$. For $t \longrightarrow (n+1)\rho_d$, system (2.2) becomes

$$\begin{aligned} x_{n+1} &= x_n + \frac{\rho_d^{\alpha_d}}{\Gamma(\alpha_d + 1)} \left(a x_n - x_n y_n\right), \\ y_{n+1} &= y_n + \frac{\rho_d^{\alpha_d}}{\Gamma(\alpha_d + 1)} \left(-b y_n + x_n^2\right). \end{aligned} \tag{2.3}$$

2.2. Stability analysis

The system (2.3) has the three equilibrium points $E(x, y) := (0, 0), (\pm\sqrt{ab}, a)$. We will discuss the dynamical properties of system (2.3) at $E_+ = (\sqrt{ab}, a)$ only.

The Jacobian matrix of the system (2.3), evaluated at $E(x^*, y^*)$, is given by:

$$J\left(x^*, y^*\right) = \begin{pmatrix} 1 + (a - y^*)\dfrac{\rho_d^{\alpha_d}}{\Gamma(\alpha_d + 1)} & -x^* \dfrac{\rho_d^{\alpha_d}}{\Gamma(\alpha_d + 1)} \\ 2x^* \dfrac{\rho_d^{\alpha_d}}{\Gamma(\alpha_d + 1)} & 1 - b\dfrac{\rho_d^{\alpha_d}}{\Gamma(\alpha_d + 1)} \end{pmatrix}.$$

At $E_+(\sqrt{ab}, a)$, the Jacobian matrix is

$$J_{E_+} = \begin{pmatrix} 1 & -\sqrt{ab}\dfrac{\rho_d^{\alpha_d}}{\Gamma(\alpha_d + 1)} \\ 2\sqrt{ab}\dfrac{\rho_d^{\alpha_d}}{\Gamma(\alpha_d + 1)} & 1 - b\dfrac{\rho_d^{\alpha_d}}{\Gamma(\alpha_d + 1)} \end{pmatrix}.$$

The characteristic equation of the matrix J_{E+} is

$$F(\lambda) := \lambda^2 - \mathrm{Tra}(\mathrm{J_{E_+}})\lambda + \mathrm{Detr}(\mathrm{J_{E_+}}) = 0,$$

where $\mathrm{Tra}(\mathrm{J_{E_+}})$ and $\mathrm{Detr}(\mathrm{J_{E_+}})$ are

$$\begin{aligned} \mathrm{Tra}(\mathrm{J_{E_+}}) &= 2 - b\frac{\rho_d^{\alpha_d}}{\Gamma(\alpha_d + 1)}, \\ \mathrm{Detr}(\mathrm{J_{E_+}}) &= 1 + b\frac{\rho_d^{\alpha_d}}{\Gamma(\alpha_d + 1)} \left(-1 + 2a\frac{\rho_d^{\alpha_d}}{\Gamma(\alpha_d + 1)}\right). \end{aligned}$$

The eigenvalues are

$$\lambda_{1,2} = \frac{1}{2}\left(2 - b\frac{\rho_d^{\alpha_d}}{\Gamma(1 + \alpha_d)} \pm \sqrt{b(-8a + b)}\frac{\rho_d^{\alpha_d}}{\Gamma(a + \alpha_d)}\right).$$

Let $\rho_{d1,d2} := \left(\Gamma(1 + \alpha_d)\dfrac{b \mp \sqrt{b(-8a+b)}}{2ab}\right)^{\frac{1}{\alpha_d}}$ and $\rho_{d3} := \left(\dfrac{\Gamma(1+\alpha_d)}{2a}\right)^{\frac{1}{\alpha_d}}$.

For the convenience of the parameter space discussion, we first present a bifurcation diagram (see Figure (1)(i)) of system (2.3) in $\mathbb{R}^2_+ := \{(\rho_d, a) | a > 0, \rho_d > 0\}$. The topological types of E_+ are stated in Theorem 2.1.

Consider the following sets

$$\begin{aligned}
\mathfrak{L}_1 &:= \{(a, b, \alpha_d, \rho_d) \in (0, \infty) \mid \rho_d = \rho_{d1}, -8a + b \geq 0\}, \\
\mathfrak{L}_2 &:= \{(a, b, \alpha_d, \rho_d) \in (0, \infty) \mid \rho_d = \rho_{d2}, -8a + b \geq 0\}, \\
\mathfrak{L}_3 &:= \{(a, b, \alpha_d, \rho_d) \in (0, \infty) \mid \rho_d = \rho_{d3}, -8a + b < 0\}.
\end{aligned}$$

Theorem 2.1. *If $(a, b, \alpha_d, \rho_d) \in \mathfrak{L}_1$ or $\mathfrak{L}_2$, then E_+ is non-hyperbolic saddle with Period-doubling. If $(a, b, \alpha_d, \rho_d) \in \mathfrak{L}_3$, then E_+ is non-hyperbolic focus.*

Conditions		E_+	Cases
$-8a + b \geq 0$	$0 < \rho_d < \rho_{d1}$	Stable node	$\mathfrak{D}_1$
	$\rho_{d1} < \rho_d < \rho_{d2}$	Saddle point with Period-doubling	$\mathfrak{D}_2$
	$\rho_d > \rho_{d2}$	Unstable node with Period-doubling	$\mathfrak{D}_3$
$-8a + b < 0$	$\rho_d > \rho_{d3}$	Unstable focus	$\mathfrak{D}_4$
	$\rho_d < \rho_{d3}$	Stable focus	$\mathfrak{D}_5$

2.3. Analysis of NS bifurcation

Consider the system (2.3) at $E(x^*, y^*)$. We choose the parameters (a, b, α_d, ρ_d) arbitarily lie in $\mathfrak{L}_3$.

So the eigenvalues of the system (2.3) are $\lambda_{1,2}(\rho_{d3}) \in \mathbb{C}$ with $|\lambda(\rho_{d3})| = 1$.

Also,

$$\begin{aligned}
&\frac{d\,|\lambda_i(\rho_d)|}{d\rho_d}|_{\rho_d=\rho_{d3}} = -\frac{b}{2} \neq 0, \\
&-(Tr(J_{E+}))|_{\rho_d=\rho_{d3}} \neq 0 \Rightarrow \frac{b - 4a}{2a} \neq 0, 1,
\end{aligned} \tag{2.4}$$

which obviously satisfy $\lambda^k(\rho_{d3}) \neq 1$ for $k = 1, 2, 3, 4$. Using $\hat{x_e} = x - x^+, \hat{y_e} = y - y^+$ and put $A(\rho_{d3}) = J(x^*, y^*)$. We take $E(x^*, y^*)$ to (0,0). So the system(2.3) can be written as

$$\begin{pmatrix} \hat{x_e} \\ \hat{y_e} \end{pmatrix} \to A(\rho_{d3}) \begin{pmatrix} \hat{x_e} \\ \hat{y_e} \end{pmatrix} + \begin{pmatrix} F_1(\hat{x_e}, \hat{y_e}, \rho_{d3}) \\ F_2(\hat{x_e}, \hat{y_e}, \rho_{d3}) \end{pmatrix}, \tag{2.5}$$

where $\tilde{X} = (\hat{x_e}, \hat{y_e})^T$ and

$$\begin{aligned}
F_1(\hat{x_e}, \hat{y_e}, \rho_{d3}) &= \frac{-\hat{x_e}\hat{y_e}}{2a}, \\
F_2(\hat{x_e}, \hat{y_e}, \rho_{d3}) &= \frac{\hat{x_e}^2}{2a}.
\end{aligned}$$

So system (2.5) can be written as

$$\tilde{X}_{n+1} = A\tilde{X}_n + \frac{1}{2}B\left(\tilde{X}_n, \tilde{X}_n\right) + \frac{1}{6}C\left(\tilde{X}_n, \tilde{X}_n, \tilde{X}_n\right) + O\left(\left\|\tilde{X}_n\right\|^4\right),$$

where the multi-linear vector functions of $x, y, u \in \mathbb{R}^2$ are defined as follows:

$$B_1(x,y) = \sum_{j,k=1}^{2} \frac{\delta^2 F_1(\xi, \rho_{d3})}{\delta\xi_j \delta\xi_k}\bigg|_{\xi=0} x_j y_k = -\frac{x_1 y_2 + x_2 y_1}{2a},$$

$$B_2(x,y) = \sum_{j,k=1}^{2} \frac{\delta^2 F_2(\xi, \rho_{d3})}{\delta\xi_j \delta\xi_k}\bigg|_{\xi=0} x_j y_k = \frac{x_1 y_1}{a},$$

and

$$C_1(x,y,u) = \sum_{j,k,l=1}^{2} \frac{\delta^2 F_1(\xi, \rho_{d3})}{\delta\xi_j \delta\xi_k \delta\xi_l}\bigg|_{\xi=0} x_j y_k u_l = 0,$$

$$C_2(x,y,u) = \sum_{j,k,l=1}^{2} \frac{\delta^2 F_1(\xi, \rho_{d3})}{\delta\xi_j \delta\xi_k \delta\xi_l}\bigg|_{\xi=0} x_j y_k u_l = 0.$$

Assume $q_1, q_2 \in \mathbb{C}^2$ be associated eigenvectors of $A(\rho_{d3})$ and $A^T(\rho_{d3})$ for eigenvalues $\lambda(\rho_{d3})$ and $\bar{\lambda}(\rho_{d3})$ respectively such that

$$A(\rho_{d3})\, q_1 = \lambda(\rho_{d3})\, q_1, \quad A(\rho_{d3})\, \bar{q_1} = \bar{\lambda}(\rho_{d3})\, \bar{q_1},$$
$$A^T(\rho_{d3})\, q_2 = \bar{\lambda}(\rho_{d3})\, q_2, \quad A^T(\rho_{d3})\, \bar{q_2} = \lambda(\rho_{d3})\, \bar{q_2},$$

and $\langle q_1, q_2 \rangle = 1$.

Using calculations, we get

$$q_1 = \begin{pmatrix} \dfrac{b + i\sqrt{(8a-b)b}}{4\sqrt{ab}} \\ 1 \end{pmatrix}, \quad q_2 = \begin{pmatrix} -\dfrac{2\sqrt{ab}(b - i\sqrt{(8a-b)}b^{1/2})}{8ab + i\sqrt{(8a-b)}b^{3/2} - b^2} \\ \dfrac{4ab}{8ab + i\sqrt{(8a-b)}b^{3/2} - b^2} \end{pmatrix}.$$

We decompose $\tilde{X} \in \mathbb{R}^2$ as $\tilde{X} = wq_1 + \bar{w}\bar{q_1}$ by choosing ρ_d vary close to ρ_{d3} with $w \in \mathbb{C}$. Then w can be written as $w = \langle q_2, X \rangle$. So the system (2.3) transformed to the given system for $|\rho_d|$ close to ρ_{d3}:

$$w \longmapsto \lambda(\rho_d) w + \widehat{g}(w, \bar{w}, \rho_d),$$

where $\lambda(\rho_d) = (1 + \widehat{\phi_d}(\rho_d))e^{i\theta(\rho_d)}$ with $\widehat{\phi_d}(\rho_{d3}) = 0$ and $\widehat{g}(w, \bar{w}, \rho_d)$ is a smooth complex-valued function. Applying Taylor expansion to $\widehat{g}$, we have

$$\widehat{g}(w, \bar{w}, \rho_d) = \sum_{k+l \geq 2} \frac{1}{k!l!} \widehat{g}_{kl}(\rho_d) w^{k-l} \quad \text{with} \quad \widehat{g}_{kl} \in \mathbb{C}, k, l = 0, 1, \ldots,$$

where

$$\widehat{g}_{20}(\rho_{d3}) = \langle q_2, B(q_1, q_1) \rangle = \frac{3\left(-4ab + i\sqrt{(8a-b)}b^{3/2} + b^2\right)}{8ab - i\sqrt{(8a-b)}b^{3/2} - b^2}\delta,$$

$$\widehat{g}_{11}(\rho_{d3}) = \langle q_2, B(q_1, \bar{q_1}) \rangle = \frac{4ab + i\sqrt{(8a-b)}b^{1/2} + b^2}{2a\left(8ab - i\sqrt{(8a-b)}b^{3/2} - b^2\right)}\delta,$$

$$\widehat{g}_{02}\left(\rho_{d3}\right)=\langle q_2,B(\bar{q}_1,\bar{q}_1)\rangle=\frac{4ab-i\sqrt{(8a-b)}b^{7/2}+b^2}{2ab^2\left(8ab-i\sqrt{(8a-b)}b^{3/2}-b^2\right)}\delta,$$
$$\widehat{g}_{21}\left(\rho_{d3}\right)=\langle q_2,C(q_1,q_1,\bar{q}_1)\rangle=0, \tag{2.6}$$

with $\frac{\rho_d^{\alpha_d}}{\Gamma(\alpha_d+1)}=\delta=\frac{1}{2a}$.

The following coefficient denoted by $\tilde{\Omega}(\rho_{d3})$, not to be zero determines the direction for NS bifurcation

$$\tilde{\Omega}(\rho_{d3})=\mathrm{Re}\left(\frac{\lambda_2\widehat{g}_{21}}{2}\right)-\mathrm{Re}\left(\frac{(1-2\lambda_1)\,{\lambda_2}^2}{2\,(1-\lambda_1)}\widehat{g}_{20}\widehat{g}_{11}\right)-\frac{1}{2}\left|\widehat{g}_{11}\right|^2-\frac{1}{4}\left|\widehat{g}_{02}\right|^2. \tag{2.7}$$

The following theorem is made regarding Neimark-Sacker bifurcation.

Theorem 2.2. *If ρ_d varies its value in small region of $\mathfrak{L}_3$ and Eq. (2.4) is true with $\tilde{\Omega}(\rho_{d3})\neq 0$ then the model (2.3) passes through a NS bifurcation at $E(x^*,y^*)$. Moreover, if $\tilde{\Omega}(\rho_{d3})<0$ (resp. $\tilde{\Omega}(\rho_{d3})>0$), then a single attractive (respectively repelling) invariant closed curve exists that bifurcates from $E(x^*,y^*)$.*

3. Reduced Lorenz system with conformable fractional derivative

3.1. Discretization process

We now discretize the model (1.5) using the PCA technique. Applying property (1.2) to system (1.5)'s first component for $t\in[n\rho_d,(n+1)\rho_d]$, we obtain

$$(t-n\rho_d)^{1-\alpha_d}\frac{dx(t)}{dt}=ax(t)-x(t)y(n\rho_d).$$

This leads to the following equation:

$$\frac{dx(t)}{dt}+\frac{y(n\rho_d)-a}{(t-n\rho_d)^{1-\alpha_d}}x(t)=0.$$

If this first-order linear differential equation is resolved with regard to $t\in[n\rho_d,t]$, it results in

$$x(t)=\frac{x(n\rho_d)}{e^{(y(n\rho_d)-a)\frac{(t-n\rho_d)^{\alpha_d}}{\alpha_d}}}.$$

The difference equation is obtained for $t\in(n+1)h$,

$$x(n+1)=\frac{x(n)}{e^{(y(n)-a)\frac{\rho_d^{\alpha_d}}{\alpha_d}}}.$$

Applying the same method to the second equation of system (1.5)

$$T_{\alpha_d}y(t)=-by(t)+x^2([\frac{t}{\rho_d}]\rho_d),$$

we get,

$$y(n+1)=\frac{(by_n-x_n^2)e^{(-b\frac{\rho_d^{\alpha_d}}{\alpha_d})}+x_n^2}{b}.$$

The conformable reduced Lorenz system can be written as

$$\begin{aligned} x_{n+1} &= \frac{x_n}{e^{(y_n-a)\frac{\rho_d^{\alpha_d}}{\alpha_d}}}, \\ y_{n+1} &= \frac{(by_n - x_n^2)e^{(-b\frac{\rho_d^{\alpha_d}}{\alpha_d})} + x_n^2}{b}. \end{aligned} \tag{3.1}$$

Remark 3.1. The Caputo fractional order discrete Lorenz model benefits complex systems by incorporating memory effects, considering both current inputs and past states. This allows for more accurate representations, especially for phenomena reliant on past events. Fractional derivatives offer greater versatility than integer-order models, crucial for ecological systems with anomalous diffusion. However, calculating these derivatives is resource-intensive and can obscure parameter significance. Research is ongoing to improve methods for solving these equations and enhance simulation stability.

Remark 3.2. Using conformable fractional derivatives in a discrete Lorenz model captures complex dynamics and unpredictability. These derivatives better represent minor characteristics and memory effects, enhancing understanding and prediction. They offer versatile modeling for real-world systems with fractional-order dynamics, improving controllability and long-term prediction. The choice depends on study goals, system properties, and interest in non-integer dynamics, providing deeper insights into the Lorenz system and leveraging fractional calculus for complex systems.

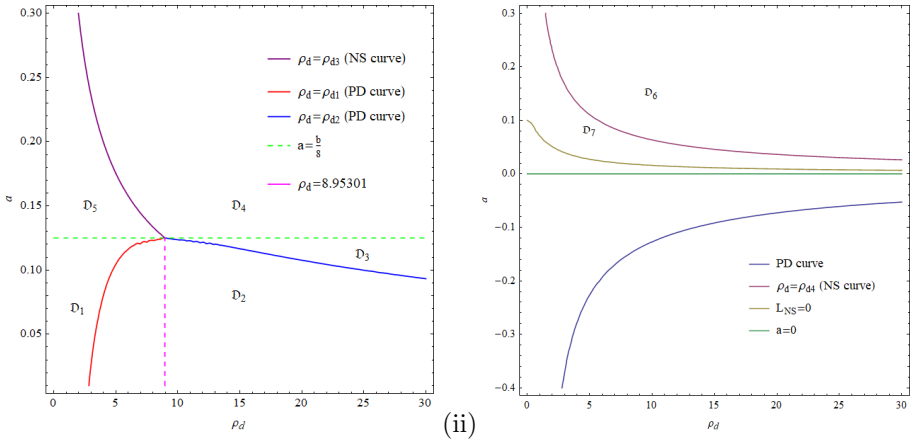

Figure 1. Bifurcation diagram of system (2.3) and (3.1) at the equilibrium point E_+ with $b = 1, \alpha_d = 0.58$.

Figure 1 shows both PD and NS bifurcations for system (2.3), while only NS bifurcation occurs for system (3.1) at the equilibrium point E_+. Fractional calculus extends derivatives and integrals to non-integer orders using two main methods: conformable and Caputo derivatives. Conformable derivatives are simpler and more intuitive but may not apply if the function doesn't meet certain requirements. Caputo derivatives offer useful integral representations for solving equations but are more complex and non-local, considering the function's entire history. The choice

between them depends on the model and system characteristics, with each having its own pros and cons.

3.2. Stability analysis

The system (3.1) has also three equilibrium points $(0,0)$ and $(\pm\sqrt{ab}, a)$ which are same as in system (2.3). The Jacobian matrix of the system (3.1), evaluated at $E(x^*, y^*)$, is given by:

$$J(x^*, y^*) = \begin{pmatrix} e^{(a-y^*)\frac{\rho_d^{\alpha_d}}{\alpha_d}} & -e^{(a-y^*)\frac{\rho_d^{\alpha_d}}{\alpha_d}} x^* \dfrac{\rho_d^{\alpha_d}}{\alpha_d} \\ \dfrac{(2-2e^{-b\frac{\rho_d^{\alpha_d}}{\alpha_d}})x^*}{b} & e^{-b\frac{\rho_d^{\alpha_d}}{\alpha_d}} \end{pmatrix}.$$

Now we have the Jacobian matrix at $E_+(\sqrt{ab}, a)$

$$J_{E_+} = \begin{pmatrix} 1 & \sqrt{ab}\dfrac{\rho_d^{\alpha_d}}{\alpha_d} \\ \dfrac{2\sqrt{a}(1-e^{-b\frac{\rho_d^{\alpha_d}}{\alpha_d}})}{\sqrt{b}} & e^{-b\frac{\rho_d^{\alpha_d}}{\alpha_d}} \end{pmatrix}.$$

The characteristic equation of the matrix J_{E_+} is

$$F(\lambda) := \lambda^2 - \mathrm{Tra}(\mathrm{J_{E_+}})\,\lambda + \mathrm{Detr}(\mathrm{J_{E_+}}) = 0,$$

where $\mathrm{Tra}(\mathrm{J_{E_+}})$ and $\mathrm{Detr}(\mathrm{J_{E_+}})$ is given by

$$\mathrm{Tra}(\mathrm{J_{E_+}}) = 1 + e^{-b\dfrac{\rho_d^{\alpha_d}}{\alpha_d}},$$
$$\mathrm{Detr}(\mathrm{J_{E_+}}) = e^{-b\frac{\rho_d^{\alpha_d}}{\alpha_d}}(1 + 2a(-1 + e^{b\frac{\rho_d^{\alpha_d}}{\alpha_d}})\frac{\rho_d^{\alpha_d}}{\alpha_d}).$$

The eigenvalues are

$$\lambda_{1,2} = \frac{e^{-b\frac{\rho_d^{\alpha_d}}{\alpha_d}}\left(\sqrt{b}(1+e^{b\frac{\rho_d^{\alpha_d}}{\alpha_d}}) \pm \sqrt{-b(-1+e^{b\frac{\rho_d^{\alpha_d}}{\alpha_d}})(1+e^{b\frac{\rho_d^{\alpha_d}}{\alpha_d}}(-1+8a\frac{\rho_d^{\alpha_d}}{\alpha_d}))}\right)}{2\sqrt{b}}.$$

Let $\rho_{d4} := \left(\frac{\alpha_d}{2a}\right)^{\frac{1}{\alpha_d}}$. The choice of ρ_{d4} is critical as it directly influences the system's stability and dynamic behavior. By carefully selecting ρ_{d4}, researchers can control the balance between chaotic and stable states, optimizing the model for specific applications. To make discussion easier, we first provide a bifurcation diagram(see Figure(1)(ii)) for system (3.1) in the parameter space $\mathbb{R}^2_+ := \{(\rho_d, a) | a > 0, \rho_d > 0\}$. The topological properties of E_+ are presented in Theorem 3.1.

Consider the following set

$$\mathfrak{L}_4 := \{(a, b, \alpha_d, \rho_d) \in (0,\infty) \mid \rho_d = \rho_{d4}, \mathfrak{L}_{NS} < 0\},$$

where $\mathfrak{L}_{NS} = -b(-1+e^{b\frac{\rho_d^{\alpha_d}}{\alpha_d}})(1+e^{b\frac{\rho_d^{\alpha_d}}{\alpha_d}}(-1+8a\frac{\rho_d^{\alpha_d}}{\alpha_d}))$.

Theorem 3.1. *If $(a, b, \alpha_d, \rho_d) \in \mathfrak{L}_4$, then E_+ is non-hyperbolic focus.*

Conditions		E_+	Cases
$\mathfrak{L}_{NS} < 0$	$\rho_d > \rho_{d4}$	Unstable focus	$\mathfrak{D}_6$
	$\rho_d < \rho_{d4}$	Stable focus	$\mathfrak{D}_7$

3.3. NS bifurcation analysis

When the parameters $(a, b, \alpha_d, \rho_d) \in \mathfrak{L}_4$, then the system (3.1) have the eigenvalues

$$\lambda, \bar{\lambda} = \frac{Tr(J_{E+}) \pm i\sqrt{4Detr(J_{E+}) - Tr(J_{E+})^2}}{2}.$$

Moreover

$$\begin{aligned} &\frac{d\,|\lambda_i(\rho_d)|}{d\rho_d}|_{\rho_d=\rho_{d4}} = -a - ae^{-\frac{b}{2a}}, \\ &-(Tr(J_{E+}))|_{\rho_d=\rho_{d4}} \neq 0, 1 \Rightarrow -1 - e^{-\frac{b}{2a}} \neq 0, 1. \end{aligned} \tag{3.2}$$

Using the transformation $\hat{x_e} = x - x^+, \hat{y_e} = y - y^+$ and set $A(\delta) = J(x^*, y^*)$. Take $E(x^*, y^*)$ to the origin. So the system (3.1) is

$$\tilde{X} = A(\rho_d)\tilde{X} + F,$$

where $\tilde{X} = (\hat{x_e}, \hat{y_e})^T$ and $F = (F_1, F_2)^T$ are given by

$$\begin{aligned} &F_1(\hat{x_e}, \hat{y_e}, \rho_{d4}) \\ &= \frac{1}{2}\left(-2\tilde{x}\tilde{y}\frac{\rho_d^{\alpha_d}}{\alpha_d} + \sqrt{ab}\tilde{y}^2(\frac{\rho_d^{\alpha_d}}{\alpha_d})^2\right) + \frac{1}{6}\left(3\tilde{x}\tilde{y}^2(\frac{\rho_d^{\alpha_d}}{\alpha_d})^2 - \sqrt{ab}\tilde{y}^3(\frac{\rho_d^{\alpha_d}}{\alpha_d})^3\right), \\ &F_2(\hat{x_e}, \hat{y_e}, \rho_{d4}) = \frac{(2 - 2e^{-b\frac{\rho_d^{\alpha_d}}{\alpha_d}})\tilde{x}^2}{2b}. \end{aligned}$$

Now

$$\begin{aligned} B_1(x, y) &= \frac{\rho_d^{\alpha_d}}{\alpha_d}\left(-x_2y_1 - x_1y_2 + \sqrt{ab}x_2y_2\frac{\rho_d^{\alpha_d}}{\alpha_d}\right), \\ B_2(x, y) &= \frac{(2 - 2e^{-b\frac{\rho_d^{\alpha_d}}{\alpha_d}}x_1y_1)}{b}, \end{aligned}$$

and

$$\begin{aligned} C_1(x, y, v) &= (\frac{\rho_d^{\alpha_d}}{\alpha_d})^2(v_1x_2y_2 + v_2(x_1y_2 + x_2(y_1 - \sqrt{ab}y_2\frac{\rho_d^{\alpha_d}}{\alpha_d}))), \\ C_2(x, y, v) &= 0. \end{aligned}$$

Assume that $q_1, q_2 \in \mathbb{C}^2$ be associated eigenvectors of $A(\rho_{d4})$ and $A^T(\rho_{d4})$ for eigenvalue $\lambda(\rho_{d4})$ and $\bar{\lambda}(\rho_{d4})$.

Direct calculation yields the following result,

$$q_1 = \begin{pmatrix} \tilde{\zeta_1} + i\tilde{\zeta_2} \\ 1 \end{pmatrix}, \quad q_2 = \begin{pmatrix} \tilde{\xi_1} + i\tilde{\xi_2} \\ 1 \end{pmatrix},$$

where

$$\tilde{\zeta_1} = \frac{\sqrt{b}}{4\sqrt{a}}, \quad \tilde{\zeta_2} = \frac{-\sqrt{b}\sqrt{(1+e^{b\frac{\rho_d^{\alpha_d}}{\alpha_d}}(-1+8a\frac{\rho_d^{\alpha_d}}{\alpha_d}))}}{4\sqrt{a}\sqrt{-1+e^{b\frac{\rho_d^{\alpha_d}}{\alpha_d}}}},$$

$$\tilde{\xi_1} = -\frac{1-e^{-b\frac{\rho_d^{\alpha_d}}{\alpha_d}}}{2\sqrt{ab}\frac{\rho_d^{\alpha_d}}{\alpha_d}}, \quad \tilde{\xi_2} = -\frac{e^{-b\frac{\rho_d^{\alpha_d}}{\alpha_d}}\sqrt{(-1+e^{b\frac{\rho_d^{\alpha_d}}{\alpha_d}})(1+e^{b\frac{\rho_d^{\alpha_d}}{\alpha_d}}(-1+8a\frac{\rho_d^{\alpha_d}}{\alpha_d}))}}{2\sqrt{ab}\frac{\rho_d^{\alpha_d}}{\alpha_d}}.$$

We take $q_2 = \gamma_{N2} q_2$ where, $\gamma_{N2} = \frac{1}{1+(\xi_1+i\xi_2)(\zeta_1-i\zeta_2)}$.
As a result, the eigenvectors are calculated as follows:

$$q_1 = \begin{pmatrix} \zeta_1 + i\zeta_2 \\ 1 \end{pmatrix}, \quad q_2 = \begin{pmatrix} \frac{\xi_1+i\xi_2}{1+(\xi_1+i\xi_2)(\zeta_1-i\zeta_2)} \\ \frac{1}{1+(\xi_1+i\xi_2)(\zeta_1-i\zeta_2)} \end{pmatrix}.$$

Also

$$\begin{aligned}
\widehat{g}_{20}(\rho_{d4}) &= \frac{-3-9e^{\frac{b}{2a}}+i\sqrt{-1-2e^{\frac{b}{2a}}+3e^{\frac{b}{a}}}}{4a+12ae^{\frac{b}{2a}}}, \\
\widehat{g}_{11}(\rho_{d4}) &= \frac{1+3e^{\frac{b}{2a}}+i\sqrt{-1-2e^{\frac{b}{2a}}+3e^{\frac{b}{a}}}}{4a+12ae^{\frac{b}{2a}}}, \\
\widehat{g}_{02}(\rho_{d4}) &= \frac{-1+6e^{\frac{b}{a}}-i\sqrt{-1-2e^{\frac{b}{2a}}+3e^{\frac{b}{a}}}+e^{\frac{b}{2a}}(-1-2i\sqrt{-1-2e^{\frac{b}{2a}}+3e^{\frac{b}{a}}})}{4a(e^{\frac{b}{2a}}+3e^{\frac{b}{a}})}, \\
\widehat{g}_{21}(\rho_{d4}) &= \frac{i\sqrt{a^3b}-i\sqrt{a^3b}e^{\frac{b}{2a}}+(a^6b^2(1+2e^{\frac{b}{2a}}-3e^{\frac{b}{a}})^2)^{\frac{1}{4}}}{8\sqrt{a^7b(-1-2e^{\frac{b}{2a}}+3e^{\frac{b}{a}})}}.
\end{aligned} \tag{3.3}$$

The following coefficient denoted by $\tilde{\Omega}(\rho_{d4})$, not to be zero determines the direction of NS bifurcation.

$$\tilde{\Omega}(\rho_{e4}) = \mathrm{Re}\left(\frac{\lambda_2\widehat{g}_{21}}{2}\right) - \mathrm{Re}\left(\frac{(1-2\lambda_1)\lambda_2{}^2}{2(1-\lambda_1)}\widehat{g}_{20}\widehat{g}_{11}\right) - \frac{1}{2}|\widehat{g}_{11}|^2 - \frac{1}{4}|\widehat{g}_{02}|^2. \tag{3.4}$$

The following theorem is made regarding Neimark-Sacker bifurcation of system (3.1).

Theorem 3.2. *If ρ_d varies its value in small region of $\mathfrak{L}_4$ and Eq. (3.2) is true with $\tilde{\Omega}(\rho_{d4}) \neq 0$ then the model (3.1) passes through a NS bifurcation at $E(x^*, y^*)$. Moreover, if $\tilde{\Omega}(\rho_{d4}) < 0$ (resp. $\tilde{\Omega}(\rho_{d4}) > 0$), then a single attractive (respectively repelling) invariant closed curve exists that bifurcates from at $E(x^*, y^*)$.*

4. Numerical study

In this part, we demonstrate some new intriguing complex dynamical behaviors present in the system (2.3) including the bifurcation diagrams, phase portraits, and Lyapunov exponents to support the earlier analytic conclusions. One well-known

method for measuring the exponential divergence of initially near-state-space trajectories is the use of maximum Lyapunov exponents, which are frequently employed to identify chaotic behavior.

4.1. Numerical example on system (2.3)

We take $a = 0.5, b = 1.0, \alpha_d = 0.58$ and ρ_d fluctuates in the range $0.7 \leq \rho_d \leq 2.2$. The equilibrium point is obtained as $E(x^*, y^*) = (0.707107, 0.5)$ and the bifurcation point is $\rho_{d3} = 0.820228$ for system (2.3).

Then $A(\rho_{d3})$ has eigenvalues $\lambda_{1,2} = 0.5 \pm 0.866025i$.

Also, we have

$$\frac{d\,|\lambda_i(\rho_d)|}{d\rho_d}|_{\rho_d=\rho_{d3}} = -\frac{b}{2} = -0.5 \neq 0,$$
$$-(Tr(J_{E+}))|_{\rho_d=\rho_{d3}} \neq 0 \Rightarrow \frac{b-4a}{2a} = -1 \neq 0, 1.$$

So, $q_1 \sim (0.288675 + 0.5i, 0.816497)^T$ and $q_2 \sim (0.816497, -0.288675 + 0.5i)^T$. And, $\gamma_{N1} = -4.16334^{-17} + 1.22474i$.

Next, by (2.6), the Taylor coefficients are given by $\widehat{g}_{20} = -1.22474 + 0.707107i$, $\widehat{g}_{11} = 0.408248 + 0.707107i$, $\widehat{g}_{02} = 0.816497 - 1.66533 \times 10^{-16}i$, $\widehat{g}_{21} = 1.16667 - 2.02073i$.

From (2.7), we have $\tilde{\Omega}(\rho_{d3}) = -1.5 < 0$. Therefore, the requirements of Theorem 2.2 are established.

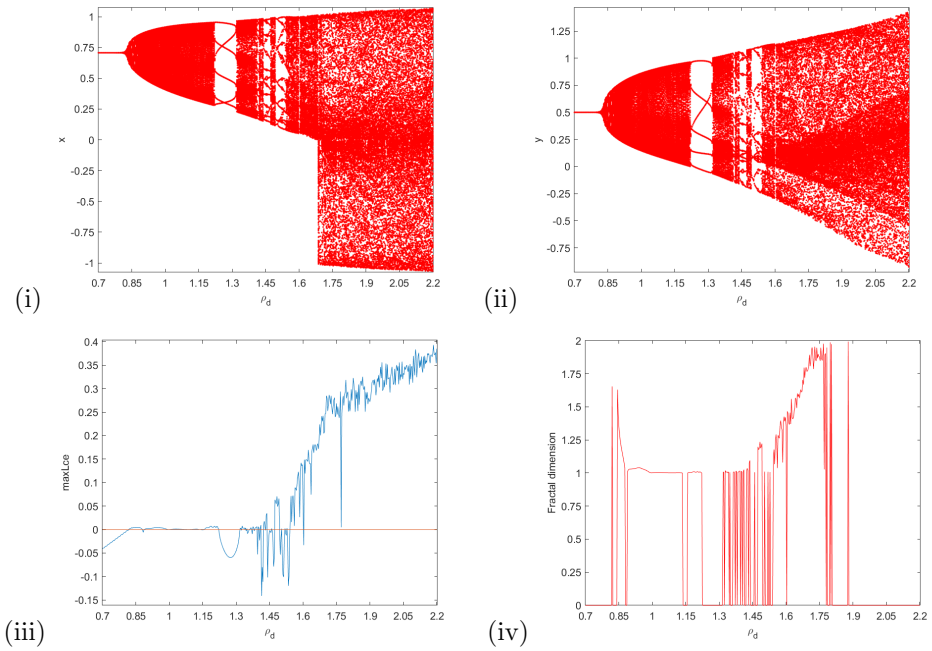

Figure 2. (i) Neimark-Sacker bifurcation in x, (ii) Neimark-Sacker bifurcation in y, (iii) maximum Lyapunov exponents, (iv) FD of system (2.3) with $a = 0.5, b = 1.0, \alpha_d = 0.58$, ρ_d varies in $0.7 \leq \rho_d \leq 2.2$ and initial conditions $(x^*, y^*) = (0.707107, 0.5)$.

The NS bifurcation diagrams are presented in Figure 2(i,ii), which demonstrates that the equilibrium point E is stable as long as $\rho_d < \rho_{d3}$, loses stability as $\rho_d = \rho_{d3}$, and displays a lovely closed invariant curve as $\rho_d > \rho_{d3}$. Unstable dynamics are compatible with the MLEs and FD (Figure 2(iii,iv)). As ρ_d rises, the closed curve abruptly disappears, and orbits with periods of $-6, -8, -13$, and -26 appear for various values of ρ_d (see Figure 3). Specifically when $\rho_d = 1.453$ an orbit appears with -26 period and at $\rho_d = 2.2$ a complete chaos in the system (2.3) happens. To emphasize the impact of using fractional derivatives, we have included bifurcation diagrams (see Figure 4 (i-iii)) for different values of α_d, specifically for $\alpha_d = 1.0$. These diagrams visually demonstrate how the system's dynamics change when fractional derivatives (with memory effects) are used instead of integer-order derivatives (without memory effects). The bifurcation diagrams demonstrate the impact of memory effects on the system's dynamics, highlighting the differences from the integer-order case. By comparing the diagrams, one can clearly see how memory effects alter the system's behavior, potentially leading to different bifurcation patterns and more complex dynamics. Figure 4(iv) displays the influence of a with fixed $\rho_d = 0.76351$. Figure 5 presents a bifurcation diagram with NS behavior, including Maximum Lyapunov Exponents (MLEs) and fractional derivatives, for system (2.3) for $a = 0.5, b = 1.0, \rho_d = 0.820228$ and α_d fluctuates in the range $0.01 \leq \alpha_d \leq 0.58$.

4.2. Numerical example on system (3.1)

We choose $a = 0.5, b = 1.0, \alpha_d = 0.58$ and ρ_d fluctuates in $0.3 \leq \rho_d \leq 4.5$. We identify a equilibrium point $E(x^*, y^*) = (0.707107, 0.5)$ and the bifurcation point is $\rho_{d4} = 0.390946$ for system (3.1).

We get $\lambda_{1,2} = 0.68394 \pm 0.729539i$ with $|\lambda_i| = 1$. Also

$$\frac{d\,|\lambda_i(\rho_d)|}{d\rho_d}|_{\rho_d=\rho_{d4}} = -a - ae^{-\frac{b}{2a}} = 0.31606 \neq 0,$$
$$-\,(Tr(J_{E+}))|_{\rho_d=\rho_{d4}} \neq 0, 1 \Rightarrow -1 - e^{-\frac{b}{2a}} = -1.36788 \neq 0, 1.$$

Let $q_1, q_2 \in \mathbb{C}^2$ be two complex eigenvectors corresponding to $\lambda_{1,2}$ respectively. Therefore, $q_1 \sim (0.264185 + 0.609799i, 0.747229)^T$ and $q_2 \sim (0.747229, -0.264185 - 0.609799i)^T$. We also have, $\gamma_{N2} = -1.00261 \times 10^{-16} + 1.09731i$. Then we get $m_1 \sim (1.21429 - 0.48969i, 1)^T$ and $m_2 \sim (-1.02105i, 0.5 + 1.23985i)^T$. The Taylor coefficients are $\widehat{g}_{20} = -1.12084 + 0.161862i$, $\widehat{g}_{11} = 0.373614 + 0.16182i$, $\widehat{g}_{02} = 0.609783 - 0.38327i$, $\widehat{g}_{21} = 0.463621 - 1.2259i$.

From (3.4), we obtain the Lyapunov coefficient $\tilde{\Omega}(\rho_{d4}) = -0.632121 < 0$. Therefore, the requirements of Theorem 3.2 are established. Figure 6 (i,ii) shows the NS bifurcation diagrams, which show that the equilibrium point is stable while $\rho_d = \rho_{d4}$, loses stability when $\rho_d < \rho_{d4}$, and exhibits an attracting closed invariant curve when $\rho_d > \rho_{d4}$. The presence of MLEs justifies system dynamics lack of stability (see Figure 6 (iii)). An invariant closed curve arises when $\rho_d > \rho_{d4}$, and as ρ_d increases higher, NS bifurcation opens a path to chaos. Figure 7 explicitly illustrates the mechanism by which an invariant smooth closed curve bifurcates from a stable equilibrium point when ρ_d changes near its critical value also by plotting the phase portraits of the system (3.1) that correspond to the bifurcation diagram shown in Figure 6 (i,ii). When $\rho_d = 0.37$ an attractor before NS bifurcation arises and at $\rho_d = 0.42$ a NS bifurcation curve occurs in the system (3.1). The figures support the findings that fractional derivatives, such as conformable fractional

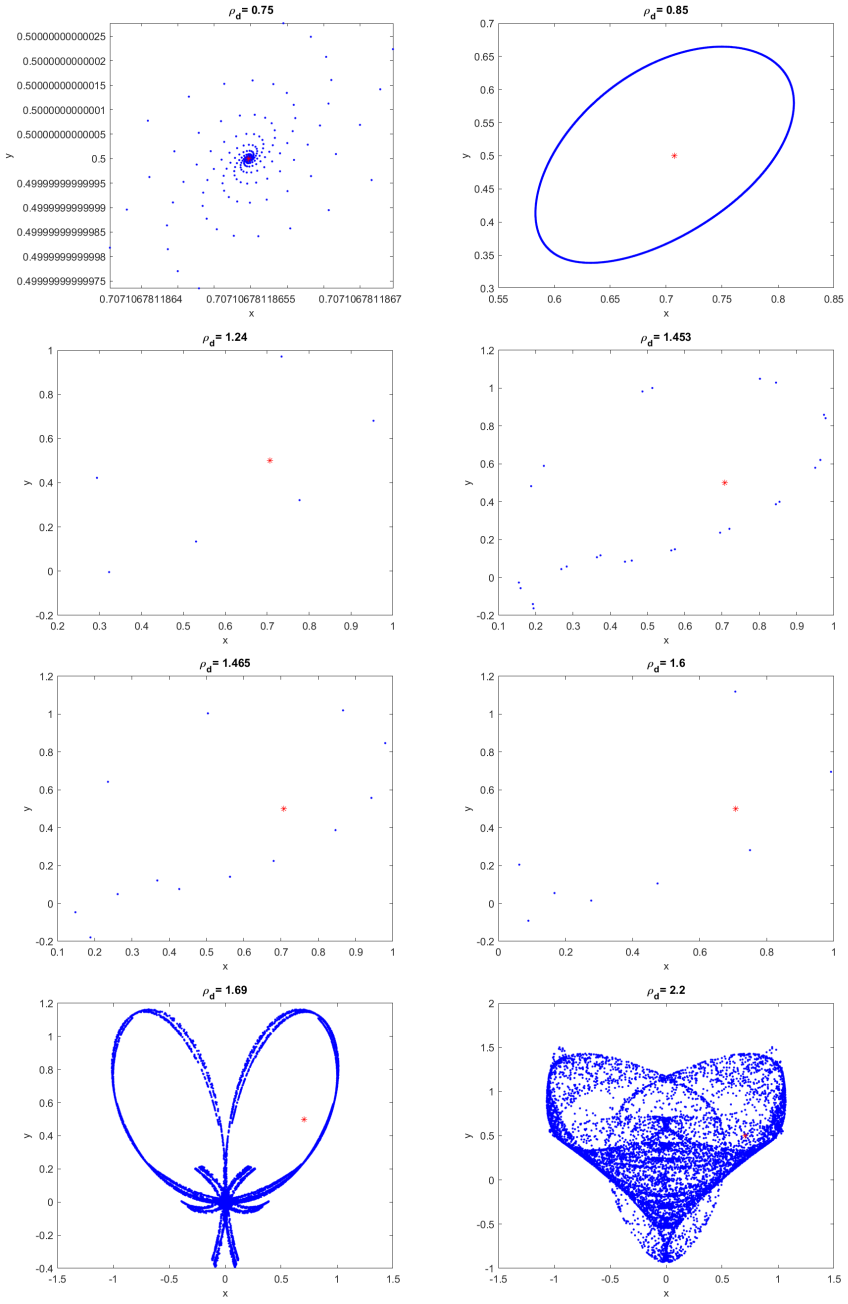

Figure 3. Phase portraits for various values of ρ_d $(\rho_d = 0.75, 0.85, 1.24, 1.453, 1.465, 1.6, 1.69, 2.2)$ corresponding to Figure 2.

derivatives, enable the inclusion of memory effects in the model. This results in a more accurate representation of systems where historical behavior influences current dynamics. The bifurcation diagrams provide a visual comparison, highlighting the significant differences and advantages of using fractional derivatives over traditional

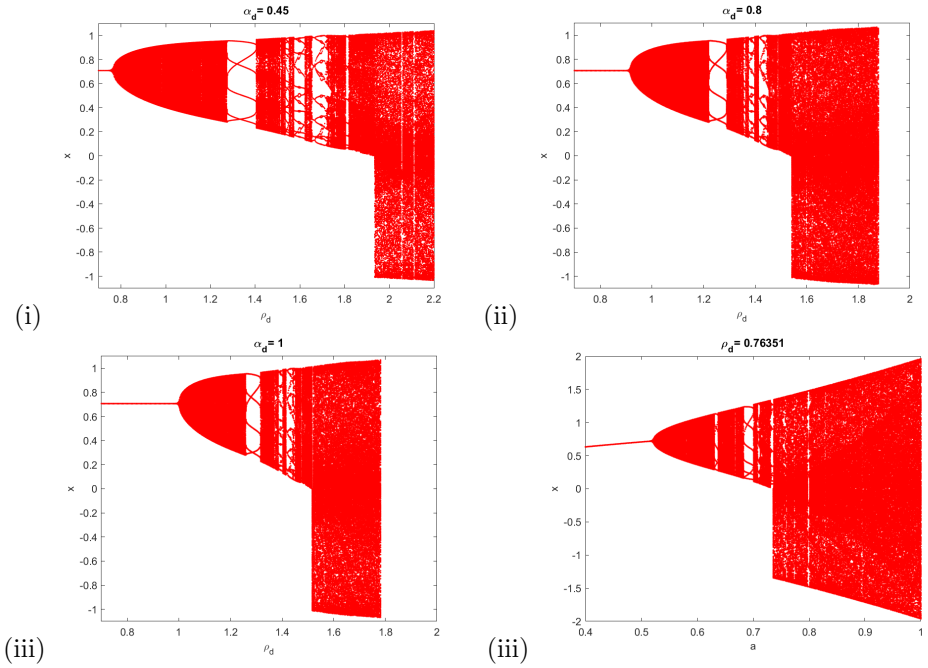

Figure 4. Neimark-Sacker bifurcation of system (2.3) in (i-iii) $x - \rho_d$ plane. For $\alpha_d < 1$, the system incorporates fractional derivatives, introducing memory effects. When $\alpha_d = 1$, the system follows traditional integer-order derivatives. (iv) Neimark-Sacker bifurcation of system (2.3) in $x - a$ plane.

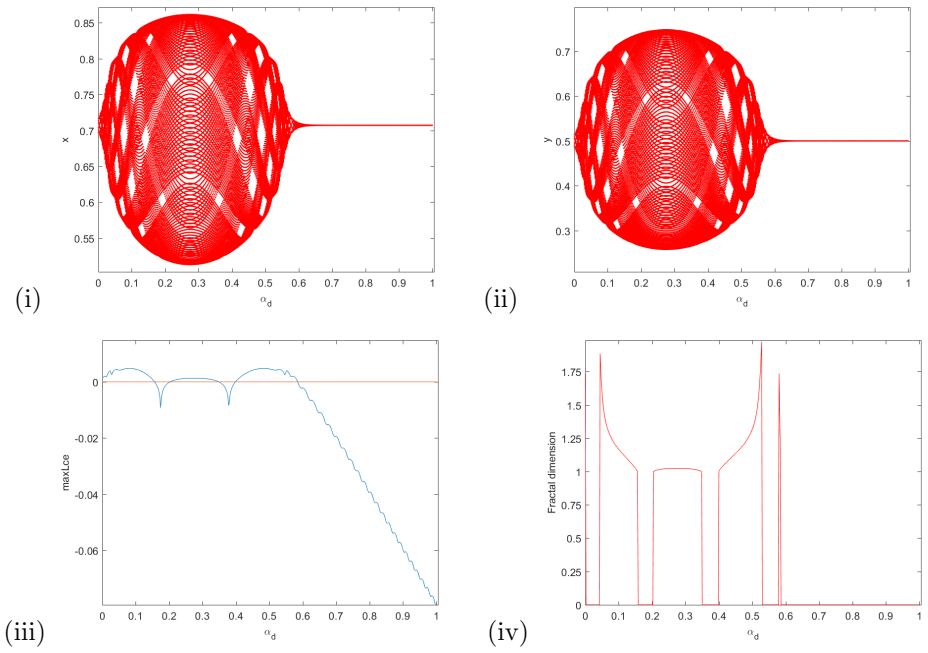

Figure 5. (i) Neimark-Sacker bifurcation in x, (ii) Neimark-Sacker bifurcation in y, (iii) maximum Lyapunov exponents, (iv) FD of system (2.3) with $a = 0.5, b = 1.0, \rho_d = 0.820228$, α_d varies in $0.01 \leq \alpha_d \leq 0.58$ and initial conditions $(x^*, y^*) = (0.707107, 0.5)$.

integer-order derivatives.

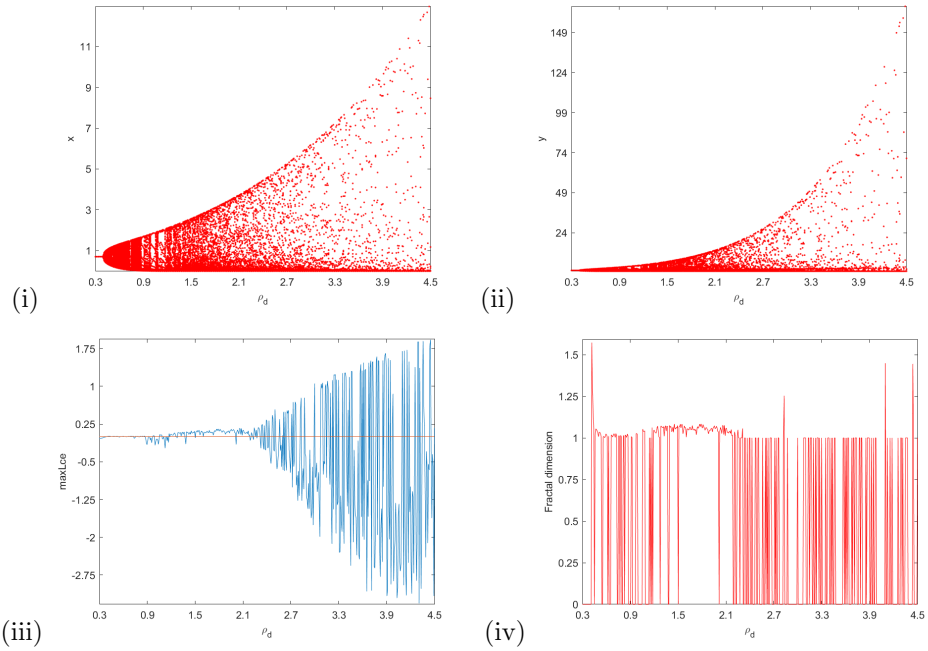

Figure 6. (i) Neimark-Sacker bifurcation in x, (ii) Neimark-Sacker bifurcation in y, (iii) maximum Lyapunov exponents, (iv) FD of system (3.1) with $a = 0.5, b = 1.0, \alpha_d = 0.58$, ρ_d varies in $0.3 \leq \rho_d \leq 4.5$ and initial conditions $(x^*, y^*) = (0.707107, 0.5)$.

4.3. Fractal dimension

To determine the chaotic attractors of a system, the fractal dimensions (FD) measurement is used and is defined by [16],

$$\widehat{D}_{LL} = k + \frac{\sum_{j=1}^{k} t_j^{**}}{|t_{k+1}^{**}|}, \tag{4.1}$$

where the largest integer k is such that $\sum_{j=1}^{k} t_j^{**} \geq 0$ and $\sum_{j=1}^{k+1} t_j^{**} < 0$ and t_j^{**}'s are Lyapunov exponenets.

Now, the fractal dimensions for the system (2.3) look like this:

$$\widehat{D}_{LL} = 2 + \frac{t_1^{**}}{|t_2^{**}|}. \tag{4.2}$$

As ρ_d increases the fractional Order reduced Lorenz system produces unstable system dynamics because the chaotic dynamics of the system (2.3) (see Figure 3) are quantified with the sign of FD (see Figure 2(iv)).

4.4. Algorithm for 0-1 Chaos Test

One technique for examining a discrete dynamical system's chaotic behavior is the 0-1 Chaos Test. Chaos in dynamical systems refers to a very sensitive dependence

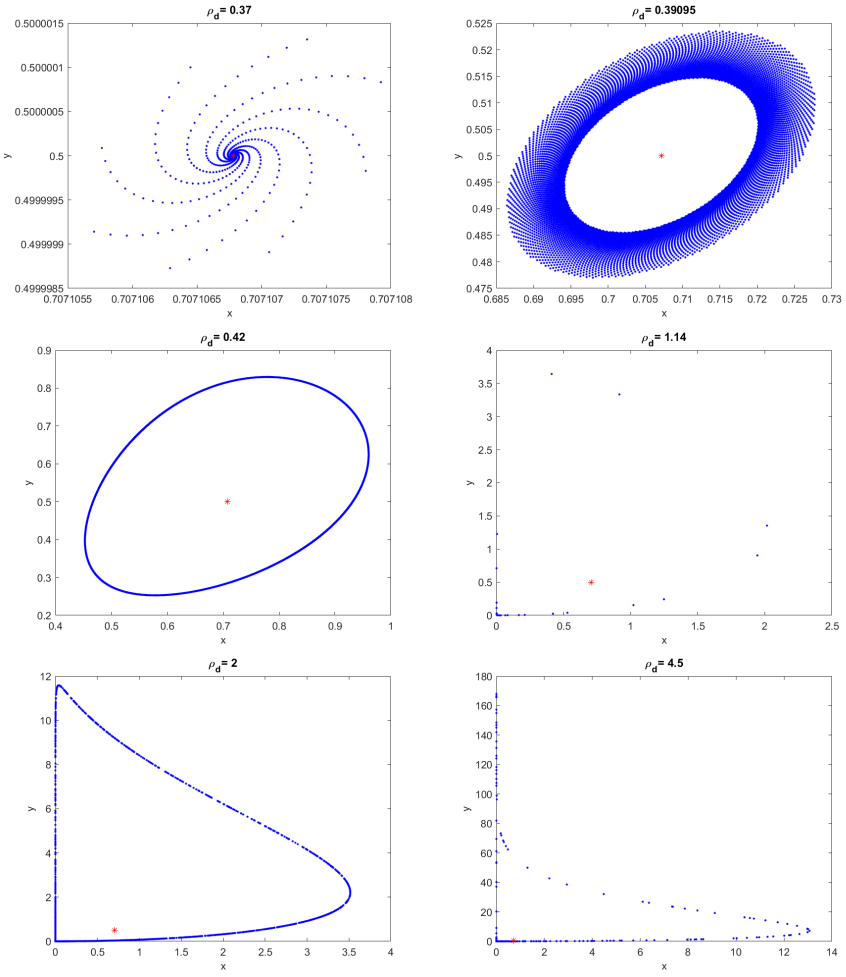

Figure 7. Phase portraits for various values of ρ_d $(\rho_d = 0.37, 0.39095, 0.42, 1.14, 2, 4.5)$ corresponding to Figure 6.

on initial conditions, where modest initial condition changes can eventually produce significantly different results. It is crucial to remember that chaos tests are a subset of chaos theory, a larger field of study that focuses on how dynamical systems behave when their beginning circumstances are extremely sensitive. Applications of chaos theory can be found in computer science, physics, biology, and economics, among other disciplines. Discrete dynamical systems can be analyzed and chaos detected using a variety of methods, one of which is the 0-1 Chaos Test. The algorithm that we followed for analyzing 0-1 chaos test is discussed in [60].

Example 4.1. Choose the values of the parameter as $a = 0.5$, $b = 1.0$, $\alpha_d = 0.58$, $\rho_d = 2.2$ with $K = 0.95999$, the Brownian-like (unbounded) trajectories in $(\widehat{q}, \widehat{w})-$plane depicted in Figure 8(a) are in harmony with a chaotic dynamic system. The correlation coefficient value is shown by the curve $\widehat{K}$ verses ρ_d in Figure 8(b). From a biological perspective, this indicates that the system is chaotic for parameter k values close to 1.

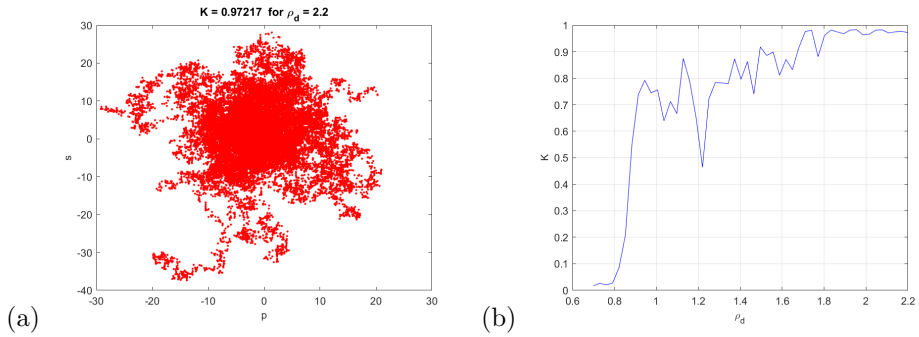

(a) (b)

Figure 8. $0-1$ choas test for model (2.3). (a) ρ versus s (b) Plot in new coordinates (ρ, K) plane.

5. Biological implications and discussion

Bifurcations in the Lorenz system can have important biological consequences when applied to the setting of physiological systems or population dynamics. The discrete simplified Lorenz model is a form of the Lorenz system that may be studied using discrete time intervals.

The Neimark-Sacker bifurcation in a discrete simplified Lorenz system might have several possible biological implications, depending on the particular setting and use of the model. The Neimark-Sacker bifurcation is linked to the change from stable periodic orbits to a torus in phase space. This may indicate the development of more intricate and semi-regular oscillating patterns in a biological setting. The Neimark-Sacker bifurcation can suggest a transition towards less regular and more complex activity patterns in systems containing biological oscillators, including cardiac or cerebral rhythms. This may be important in comprehending certain abnormalities in physiological systems. The presence of Neimark-Sacker bifurcations adds dynamic complexity to the system. In neuroscience, the Neimark-Sacker bifurcation may indicate a shift towards more intricate patterns of neuronal firing or synchronization, potentially impacting how information is processed in the brain. Systems close to a Neimark-Sacker bifurcation point can respond to parameter variations. This sensitivity could potentially affect the strength or flexibility of biological systems. Under certain circumstances, the Neimark-Sacker bifurcation can be followed by a path to chaos. This shift towards chaos could have implications for the foreseeability and steadiness of biological systems.

It is worth mentioning that the biological consequences of Neimark-Sacker bifurcations will vary based on the precise parameters of the discrete reduced Lorenz system and the applicability of the model to the biological phenomenon of interest. In-depth examination and understanding are required to make significant inferences about the effect on living organisms.

6. Chaos control

Nonlinear dynamical systems that exhibit noise-like behavior are collectively called "chaos". There are many periodic points and orbits that make up chaos, which is indesomposable and highly reliant on the initial condition. Many academics have

recently shown a keen interest in controlling chaos in discrete systems. Chaos control techniques in the discrete fractional-order reduced Lorenz model play a vital role in regulating the system's chaotic dynamics, which can otherwise lead to instability. The reduced Lorenz model, a simplified version of the full Lorenz system, still exhibits chaotic characteristics, and incorporating fractional-order dynamics increases the system's complexity. The Lorenz system is widely known for its chaotic behavior, and adding fractional-order terms introduces memory and hereditary effects, making chaotic oscillations even more unpredictable. Chaos control techniques stabilize these chaotic behaviors, preventing the system from displaying extreme, erratic patterns. By implementing chaos control, researchers and engineers can harness the complex dynamics of discrete fractional-order reduced Lorenz models while avoiding the negative effects of chaos, resulting in more reliable and practical applications.

In discrete-time systems, chaos control can be achieved in a number of ways. We introduce OGY [19], hybrid control [64], and state feedback [42] strategies for chaos control in fractional order Caputo and conformable reduced Lorenz models. When evaluating state feedback, hybrid control techniques, and the Ott-Grebogi-Yorke (OGY) chaos control method for discrete fractional-order reduced Lorenz systems, the optimal choice is largely determined by the application's specific requirements. State feedback is best suited to applications where simplicity and immediate control are essential, as it allows for direct control by adjusting corrective actions based on the system's current state, making it effective for quickly stabilizing chaotic systems. Hybrid control techniques, on the other hand, provide enhanced flexibility and adaptability, making them particularly valuable in complex and highly nonlinear systems such as the fractional-order Lorenz model. This approach combines multiple control strategies, allowing for method-switching based on the system's behavior and achieving robust performance even under significant disturbances or changing conditions. The OGY chaos control method is ideal in situations where minimal intervention is preferred. By applying small, carefully-timed adjustments near unstable periodic orbits, OGY control effectively stabilizes chaos while maintaining the system's natural dynamics. To summarize, state feedback is favored for its simplicity and user-friendliness, hybrid control is chosen for its adaptability and resilience in complex environments, and OGY control is suitable for precise, minimal intervention in discrete chaotic systems. Ultimately, the choice of technique depends on the specific needs of the application, system complexity, and desired control level. We cannot use ρ_d as a parameter in the OGY technique for controlling chaos. To implement the OGY approach, a serves as a control parameter.

We write the system (2.3) as

$$\begin{aligned} x_{n+1} &= x_n + \frac{\rho_d^{\alpha_d}}{\Gamma(\alpha_d+1)}\left(ax_n - x_n y_n\right) = \tilde{f_{1e}}(x,y,a), \\ y_{n+1} &= y_n + \frac{\rho_d^{\alpha_d}}{\Gamma(\alpha_d+1)}\left(-by_n + x_n^2\right) = \tilde{f_{2e}}(x,y,a), \end{aligned} \tag{6.1}$$

where a is the parameter for chaos control. Additionally, it is conceivable that the chaotic regions of $|a - a_0| < \tilde{\nu_e}$, where $\tilde{\nu_e} > 0$ and a_0 represent the nominal parameter, are defined by the expression $|a-a_0| < \tilde{\nu_e}$. A stabilizing feedback control technique moves the trajectory toward the desired orbit. The system (6.1) can be approximated by the following linear map in the region surrounding the unstable

equilibrium point at (x^+, y^+),

$$\begin{bmatrix} x_{n+1} - x^+ \\ y_{n+1} - y^+ \end{bmatrix} \approx \tilde{A_{ee1}} \begin{bmatrix} x_n - x^+ \\ y_n - y^+ \end{bmatrix} + \tilde{B_{ee1}} \left[a - a_0 \right], \tag{6.2}$$

where

$$\tilde{A_{ee1}} = \begin{bmatrix} \dfrac{\partial \tilde{f_{1e}}(x,y,a)}{\partial x} & \dfrac{\partial \tilde{f_{1e}}(x,y,a)}{\partial y} \\ \dfrac{\partial \tilde{f_{2e}}(x,y,a)}{\partial x} & \dfrac{\partial \tilde{f_{2e}}(x,y,a)}{\partial y} \end{bmatrix} = \begin{bmatrix} 1 & -\sqrt{a}\sqrt{b}\dfrac{\rho_d^{\alpha_d}}{\Gamma(\alpha_d+1)} \\ 2\sqrt{ab}\dfrac{\rho_d^{\alpha_d}}{\Gamma(\alpha_d+1)} & 1 - b\dfrac{\rho_d^{\alpha_d}}{\Gamma(\alpha_d+1)} \end{bmatrix},$$

and

$$\tilde{B_{ee1}} = \begin{bmatrix} \dfrac{\partial \tilde{f_{1e}}(x,y,a)}{\partial a} \\ \dfrac{\partial \tilde{f_{2e}}(x,y,a)}{\partial a} \end{bmatrix} = \begin{bmatrix} \sqrt{ab}\dfrac{\rho_d^{\alpha_d}}{\Gamma(\alpha_d+1)} \\ 0 \end{bmatrix},$$

$$\tilde{C_{ee1}} = \left[\tilde{B_{ee1}} : \tilde{A_{ee1}}\tilde{B_{ee1}} \right] = \begin{bmatrix} \sqrt{ab}\dfrac{\rho_d^{\alpha_d}}{\Gamma(\alpha_d+1)} & \sqrt{ab}\dfrac{\rho_d^{\alpha_d}}{\Gamma(\alpha_d+1)} \\ 0 & 2ab\left(\dfrac{\rho_d^{\alpha_d}}{\Gamma(\alpha_d+1)}\right)^2 \end{bmatrix}.$$

The rank of $\tilde{C_{ee1}}$ is thus readily discernible as 2. Assume that $[a - a_0] = -\tilde{K_{ee1}} \begin{bmatrix} x_n - x^+ \\ y_n - y^+ \end{bmatrix}$ where $\tilde{K_{ee1}} = [\tilde{\sigma_{ee1}} \quad \tilde{\sigma_{ee2}}]$, then system (6.1) becomes

$$\begin{bmatrix} x_{n+1} - x^+ \\ y_{n+1} - y^+ \end{bmatrix} \approx [\tilde{A_{ee1}} - \tilde{B_{ee1}}\tilde{K_{ee1}}] \begin{bmatrix} x_n - x^+ \\ y_n - y^+ \end{bmatrix}.$$

Moreover, system (2.3) offers the appropriate controlled system,

$$\begin{aligned} x_{n+1} &= x_n + \frac{\rho_d^{\alpha_d}}{\Gamma(\alpha_d+1)} \left((a_0 - \tilde{\sigma_{ee1}}(x_n - x^+) - \tilde{\sigma_{ee2}}(y_n - y^+))x_n - x_n y_n \right), \\ y_{n+1} &= y_n + \frac{\rho_d^{\alpha_d}}{\Gamma(\alpha_d+1)} \left(-by_n + x_n^2 \right). \end{aligned} \tag{6.3}$$

Furthermore, the equilibrium point is locally asymptotically stable if and only if the eigenvalues of the above matrices are situated inside an open unit disk.

Also,

$$\begin{aligned} &\tilde{A_{ee1}} - \tilde{B_{ee1}}\tilde{K_{ee1}} \\ &= \begin{bmatrix} 1 - \sqrt{ab}\dfrac{\rho_d^{\alpha_d}}{\Gamma(\alpha_d+1)}\tilde{\sigma_{ee1}} & -\sqrt{ab}\dfrac{\rho_d^{\alpha_d}}{\Gamma(\alpha_d+1)} - \sqrt{ab}\dfrac{\rho_d^{\alpha_d}}{\Gamma(\alpha_d+1)}\tilde{\sigma_{ee2}} \\ 2\sqrt{ab}\dfrac{\rho_d^{\alpha_d}}{\Gamma(\alpha_d+1)} & 1 - b\dfrac{\rho_d^{\alpha_d}}{\Gamma(\alpha_d+1)} \end{bmatrix}. \end{aligned}$$

The Jacobian matrix $(A_{ee1}^{\sim}-B_{ee1}^{\sim}K_{ee1}^{\sim})$ has the following characteristic equation:

$$\begin{aligned}
&\lambda_e{}^2-\left(2-\left(b+\sqrt{ab}\sigma_{ee1}^{\sim}\right)\frac{\rho_d^{\alpha_d}}{\Gamma(\alpha_d+1)}\right)\lambda_e\\
&+1-b\frac{\rho_d^{\alpha_d}}{\Gamma(\alpha_d+1)}+2ab(1+\sigma_{ee2}^{\sim})\left(\frac{\rho_d^{\alpha_d}}{\Gamma(\alpha_d+1)}\right)^2\\
&+\sqrt{ab}\frac{\rho_d^{\alpha_d}}{\Gamma(\alpha_d+1)}\left(-1+b\frac{\rho_d^{\alpha_d}}{\Gamma(\alpha_d+1)}\right)\sigma_{ee1}^{\sim}=0.
\end{aligned}\tag{6.4}$$

If we take into account the eigenvalues (λ_{e1} and λ_{e2}) of the characteristic equation (6.4), we obtain

$$\begin{aligned}
\lambda_{e1}+\lambda_{e2}&=\left(2-\left(b+\sqrt{ab}\sigma_{ee1}^{\sim}\right)\frac{\rho_d^{\alpha_d}}{\Gamma(\alpha_d+1)}\right),\\
\lambda_{e1}\lambda_{e2}&=1-b\frac{\rho_d^{\alpha_d}}{\Gamma(\alpha_d+1)}+2ab(1+\sigma_{ee2}^{\sim})\left(\frac{\rho_d^{\alpha_d}}{\Gamma(\alpha_d+1)}\right)^2\\
&\quad+\sqrt{ab}\frac{\rho_d^{\alpha_d}}{\Gamma(\alpha_d+1)}\left(-1+b\frac{\rho_d^{\alpha_d}}{\Gamma(\alpha_d+1)}\right)\sigma_{ee1}^{\sim}.
\end{aligned}\tag{6.5}$$

The lines of marginal stability can then be obtained by solving the equations $\lambda_{e1}=\pm1$ and $\lambda_{e1}\lambda_{e2}=1$. These constraints also guarantee that λ_{e1} and λ_{e2} are inside the open unit disk. Assume $\lambda_{e1}\lambda_{e2}=1$ and from (6.5), we get

$$\begin{aligned}
K_{e1}&=\sqrt{ab}\frac{\rho_d^{\alpha_d}}{\Gamma(\alpha_d+1)}\left(-1+b\frac{\rho_d^{\alpha_d}}{\Gamma(\alpha_d+1)}\right)\sigma_{ee1}^{\sim}\\
&\quad+b\frac{\rho_d^{\alpha_d}}{\Gamma(\alpha_d+1)}\left(-1+2a(1+\sigma_{ee2}^{\sim})\frac{\rho_d^{\alpha_d}}{\Gamma(\alpha_d+1)}\right).
\end{aligned}$$

Next consider $\lambda_{e1}=1$, we obtain

$$K_{e2}=\sqrt{a}b^{\frac{3}{2}}\left(\frac{\rho_d^{\alpha_d}}{\Gamma(\alpha_d+1)}\right)^2\sigma_{ee1}^{\sim}+2ab\left(\frac{\rho_d^{\alpha_d}}{\Gamma(\alpha_d+1)}\right)^2(1+\sigma_{ee2}^{\sim}).$$

Last but not least, if $\lambda_{e1}=-1$, then

$$\begin{aligned}
&K_{e3}\\
=&\sqrt{ab}\frac{\rho_d^{\alpha_d}}{\Gamma(\alpha_d+1)}\left(2-b\frac{\rho_d^{\alpha_d}}{\Gamma(\alpha_d+1)}\right)\sigma_{ee1}^{\sim}\\
&-2\left(2+b\frac{\rho_d^{\alpha_d}}{\Gamma(\alpha_d+1)}\left(-1+a\frac{\rho_d^{\alpha_d}}{\Gamma(\alpha_d+1)}\right)+ab\left(\frac{\rho_d^{\alpha_d}}{\Gamma(\alpha_d+1)}\right)^2\sigma_{ee2}^{\sim}\right).
\end{aligned}$$

The $\sigma_{ee1}^{\sim}\sigma_{ee2}^{\sim}$ plane encircled by K_{e1},K_{e2},K_{e3} contains the stable eigenvalues are located in the bounded region for a specific set of parameter values.

Next, a hybrid control technique is used in the system (2.3) to control chaos. Our uncontrolled system (2.3) is rewritten as

$$X_{n+1}=G(X_n,\delta),\tag{6.6}$$

where $X_n \in \mathbb{R}^2$, the bifurcation parameter is $\delta \in \mathbb{R}$, and $G(.)$ is a nonlinear vector function. By imposing a hybrid control technique, the Eq. (6.6) becomes

$$X_{n+1} = \omega_e G(X_n, \delta) + (1 - \omega_e) X_n, \tag{6.7}$$

where $0 < \omega_e < 1$. At this moment, by imposing the control technique discussed previously to system (2.3), we provide the system below

$$\begin{aligned} x_{n+1} &= \omega_e \left(x_n + \frac{\rho_d^{\alpha_d}}{\Gamma(\alpha_d + 1)} \left(a x_n - x_n y_n \right) \right) + (1 - \omega_e) x_n, \\ y_{n+1} &= \omega_e \left(y_n + \frac{\rho_d^{\alpha_d}}{\Gamma(\alpha_d + 1)} \left(-b y_n + x_n^2 \right) \right) + (1 - \omega_e) y_n. \end{aligned} \tag{6.8}$$

At the point where the system's (2.3) unstable trajectories are at their most advanced, chaos is stabilized using a technique known as state feedback control. By introducing a feedback control law as the control force u_{ee} and using the following formula, system (2.3) may be made to take on a controlled form.

$$\begin{aligned} x_{n+1} &= x_n + \frac{\rho_d^{\alpha_d}}{\Gamma(\alpha_d + 1)} \left(a x_n - x_n y_n \right) + u_{ee}, \\ y_{n+1} &= y_n + \frac{\rho_d^{\alpha_d}}{\Gamma(\alpha_d + 1)} \left(-b y_n + x_n^2 \right), \\ u_{ee} &= -k_1 (x_n - x^+) - k_2 (y_n - y^+), \end{aligned} \tag{6.9}$$

where the positive equilibrium point of the system (2.3) is represented by (x^+, y^+) and k_1 and k_2 denote the feedback gains.

Example 6.1. We use $(a_0, b, \alpha_d, \rho_d) = (0.15, 1.8, 0.58, 0.53145)$ for OGY method. The system (2.3) has a equilibrium point $(x^+, y^+) = (1.95, 0.473373)$. Then,

$$\begin{aligned} & x_{n+1} \\ &= x_n + 0.777474 \left((0.15 - \sigma_{\tilde{ee}1}(x_n - 1.95) - \sigma_{\tilde{ee}2}(y_n - 0.473373)) - x_n + x_n^2 y_n \right), \\ y_{n+1} &= y_n + 0.777474 \left(1.8 - x_n^2 y_n \right), \end{aligned} \tag{6.10}$$

where $\tilde{K} = [\sigma_{\tilde{ee}1} \quad \sigma_{\tilde{ee}2}]$ serve as the gain matrix. We also get,

$$A_{\tilde{ee}1} = \begin{bmatrix} 1.65786 & 2.95634 \\ -1.43534 & -1.95634 \end{bmatrix},$$

$$B_{\tilde{ee}1} = \begin{bmatrix} 0.777474 \\ 0 \end{bmatrix},$$

$$C_{\tilde{ee}1} = \begin{bmatrix} 0.777474 & 1.28895 \\ 0 & -1.11594 \end{bmatrix},$$

and

$$A_{\tilde{ee}1} - B_{\tilde{ee}1} K_{\tilde{ee}1} = \begin{bmatrix} 1.65786 - 0.777474\sigma_{\tilde{ee}1} & 2.95634 - 0.777474\sigma_{\tilde{ee}2} \\ -1.43534 & -1.95634 \end{bmatrix}.$$

For marginal stability, the lines K_{e1}, K_{e2} and K_{e3} are provided by:

$$K_{e1} = -0.000000986495 + 1.52101\tilde{\sigma_{ee1}} - 1.11594\tilde{\sigma_{ee2}} = 0,$$
$$K_{e2} = 1.70152 + 0.743533\tilde{\sigma_{ee1}} - 1.11594\tilde{\sigma_{ee2}} = 0,$$
$$K_{e3} = -2.29848 - 2.29848\tilde{\sigma_{ee1}} + 1.11594\tilde{\sigma_{ee2}} = 0.$$

The system (6.10) stable region is displayed in Figure 9. To eliminate chaotic behavior, we use a hybrid control strategy, and all the parameters are the same as in Example 6.1 except $\rho_d = 0.5812 > \rho_{d3}$. For consequence, the equilibrium point $E(1.95, 0.473373)$ of system (2.3) is unstable, however the controlled system (6.9) is stable at this equilibrium point iff $0 < \omega_e < 0.9494221636969571$. When $\omega_e = 0.85$, the controlled system (6.9) becomes a sink. The stable region and stable trajectories are shown in Figure 9. We also show the NS bifurcation diagrams (see Figure 10) of the system (6.8) for various values of ω_e, demonstrating that the system is under control when $\omega_e = 0.58$.

We have run numerical simulations (in Figure 9) to examine the operation of the feedback control method to control of chaos in an unstable condition. The parameter values will be the same as we chose for the OGY method. The feedback gains are chosen as $k_1 = -0.42$ and $k_2 = -0.35$. In Figure 10, we also demonstrate how the state feedback approach is used to control a conformable reduced Lorenz system.

7. Conclusion

This study compares the dynamical behaviors of the discrete Caputo and conformable fractional order models. According to theoretical and numerical findings, both models have the same equilibrium points and display similar dynamical features, such as a stable steady state, periodic and quasi-periodic conditions, and NS bifurcation. We find that the increased value of α_d influences the delay of NS bifurcation of the system. The solution in fractional-order systems continuously depends on all the prior states. Therefore, utilizing fractional order α_d can aid in reducing errors caused by ignored parameters. We also determine whether chaos exists by calculating MLEs and FDs. The NS bifurcation causes the system to swiftly change from steady to chaotic dynamical behavior by forging paths from periodic and quasi-periodic states. Alternately, chaotic dynamics could develop or disappear simultaneously as bifurcations. The presence of different bifurcations from different perspectives reveals the changing behaviour of the given system as its complexity varies. For instance, the NS bifurcation sets off a path toward chaos by creating a lively shift from a stable state to interesting cycles, forming intricate dynamics such as chaotic attractors and periodic windows. Environmental changes can lead populations with unpredictable fluctuations to abruptly shift to populations with predictable fluctuations. Important information about nonlinear systems can be obtained from the invariant curve in the supercritical Neimark-Sacker bifurcation. Understanding the transition from a regular state to complicated behaviour is crucial as it reveals the system's response to parameter variations. Additionally, we apply OGY, hybrid, and state feedback control strategies to mitigate unstable system trajectories.

Our main conclusion is that the memory parameter α_d greatly affects the system's behavior. A value of α_d near 0 indicates weak memory and causes chaos, while

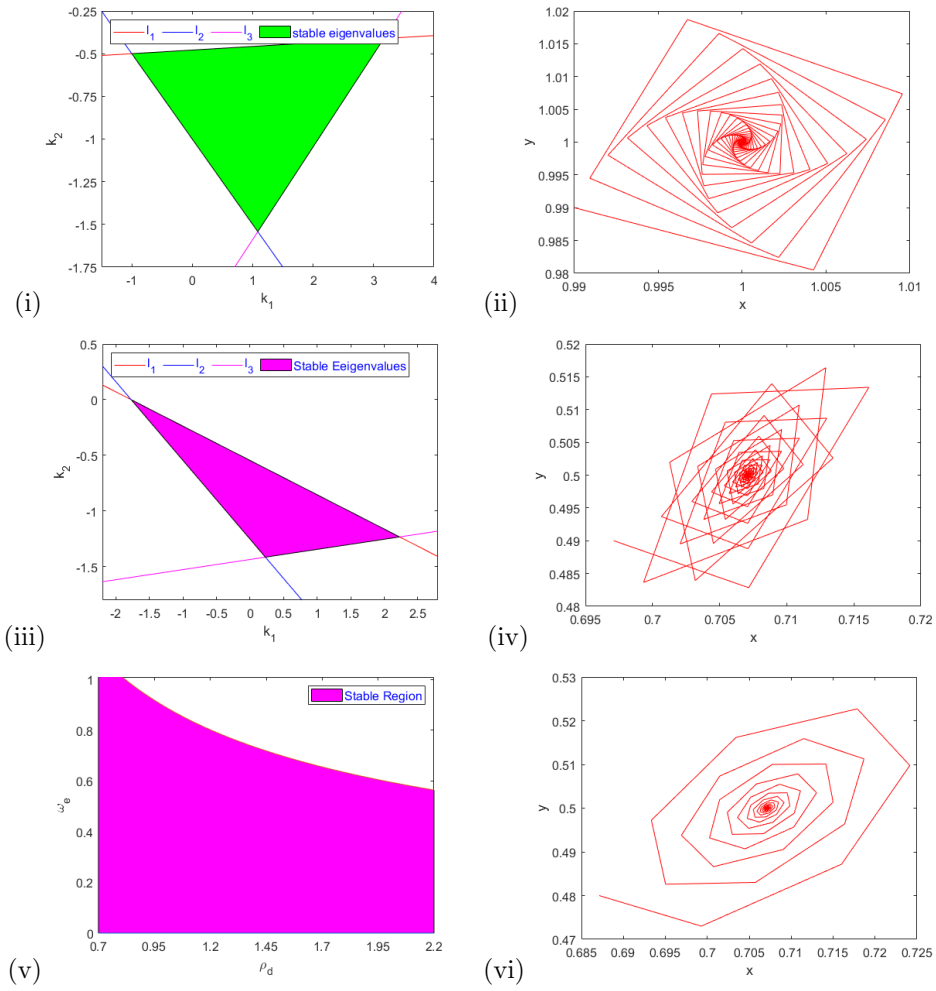

Figure 9. Stable region and trajectory of controlled Caputo reduced Lorenz system, (i-ii) OGY approach system (6.3), (iii-iv) hybrid method system (6.8), (v-vi) state feedback method system (6.9).

a value near 1 indicates strong memory and stabilizes the system. This highlights the vital role of memory in the model's behavior.

In the future, various fractional operators such as Caputo-Fabrizio, Atangana-Caputo, and others can be applied to further explore the intricate dynamic behaviors of the model. Also, investigating resonance bifurcation in the model will be a great job.

Funding. This research project is not funded.

Data and materials availability. No data were used to support this study.

Competing interests. There are no competing interests, according to the authors.

Acknowledgements. The author wishes to thank the editor and referees for their valuable comments.

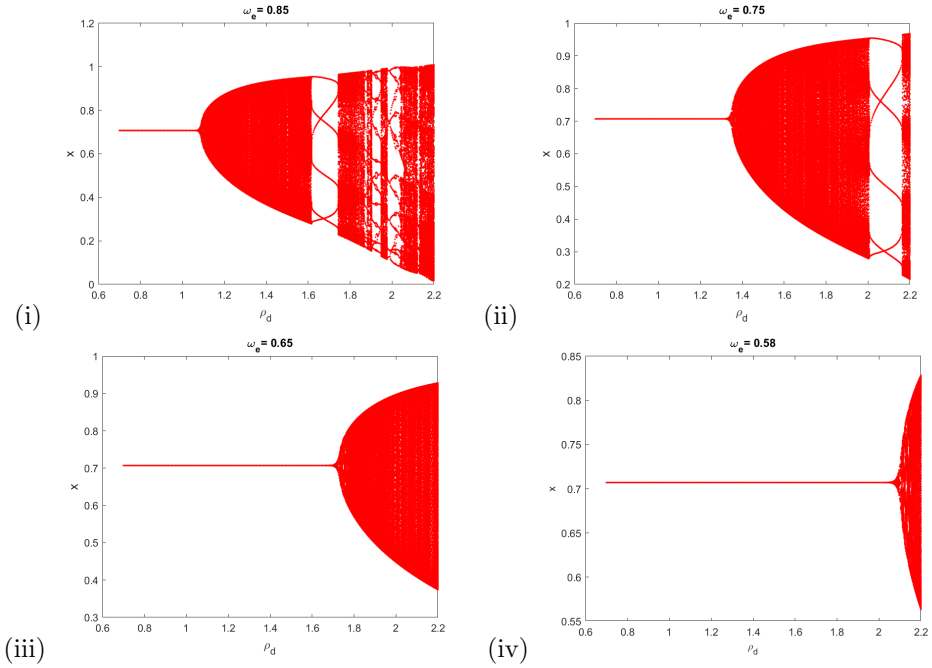

Figure 10. Neimark-Sacker bifurcation of the control system (6.8) in x for (i) $\omega_e = 0.85$, (ii) $\omega_e = 0.75$, (iii) $\omega_e = 0.65$, (iv) $\omega_e = 0.58$.

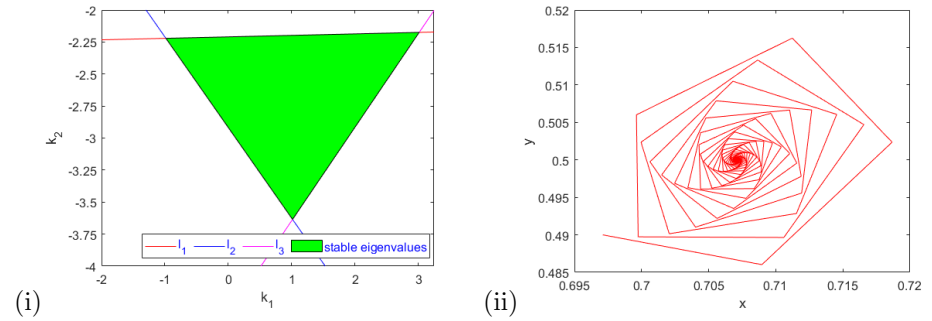

Figure 11. Stable region and trajectory of controlled conformable reduced Lorenz system.

References

[1] M. A. M. Abdelaziz, A. I. Ismail, F. A. Abdullah and M. H. Mohd, *Codimension one and two bifurcations of a discrete-time fractional-order SEIR measles epidemic model with constant vaccination*, Chaos, Solitons & Fractals, 2020, 140, 110104.

[2] M. A. M. Abdelaziz, A. I. Ismail, F. Abdullah and M. H. Mohd, *Bifurcations and chaos in a discrete SI epidemic model with fractional order*, Advances in Difference Equations, 2018, 2018(1), 1–19.

[3] R. P. Agarwal, A. El-Sayed and S. M. Salman, *Fractional-order Chua's system: Discretization, bifurcation and chaos*, Advances in Difference Equations, 2013,

1(2013), 1–13.

[4] H. N. Agiza, E. M. Elabbasy, H. El-Metwally and A. A. Elsadany, *Chaotic dynamics of a discrete prey–predator model with Holling type II*, Nonlinear Analysis: Real World Applications, 2009, 10(1), 116–129.

[5] W. M. Ahmad and J. C. Sprott, *Chaos in fractional-order autonomous nonlinear systems*, Chaos, Solitons & Fractals, 2003, 16(2), 339–351.

[6] R. Ahmed, N. Tahir and N. A. Shah, *An analysis of the stability and bifurcation of a discrete-time predator–prey model with the slow–fast effect on the predator*, Chaos: An Interdisciplinary Journal of Nonlinear Science, 2024, 34, 3.

[7] S. Akhtar, R. Ahmed, M. Batool, N. A. Shah and J. D. Chung, *Stability, bifurcation and chaos control of a discretized Leslie prey-predator model*, Chaos, Solitons & Fractals, 2021, 152, 111345.

[8] I. Ameen and P. Novati, *The solution of fractional order epidemic model by implicit Adams methods*, Applied Mathematical Modelling, 2017, 43, 78–84.

[9] A. Atangana, *A novel model for the lassa hemorrhagic fever: Deathly disease for pregnant women*, Neural Computing and Applications, 2015, 26(8), 1895–1903.

[10] R. L. Bagley and R. Calico, *Fractional order state equations for the control of visco–elastically damped structures*, Journal of Guidance, Control, and Dynamics, 1991, 14(2), 304–311.

[11] E. Balcı, S. Kartal and İ. Öztürk, *Comparison of dynamical behavior between fractional order delayed and discrete conformable fractional order tumor-immune system*, Mathematical Modelling of Natural Phenomena, 2021, 16(3).

[12] E. Balcı, İ. Öztürk and S. Kartal, *Dynamical behaviour of fractional order tumor model with Caputo and conformable fractional derivative*, Chaos, Solitons & Fractals, 2019, 123, 43–51.

[13] D. Baleanu, A. Jajarmi, E. Bonyah and M. Hajipour, *New aspects of poor nutrition in the life cycle within the fractional calculus*, Advances in Difference Equations, 2018, 2018(1), 1–14.

[14] N. S. S. Barhoom and S. Al-Nassir, *Discretization fractional-order biological model with optimal harvesting*, Abstract and Applied Analysis, 2022, 2022. DOI: 10.1155/2022/8171037.

[15] L. Bolton, A. Cloot, H. Alain, S. W. Schoombie, J. Slabbert and P. Jacobus, *A proposed fractional-order Gompertz model and its application to tumour growth data*, Mathematical Medicine and Biology: A Journal of the IMA, 2015, 32(2), 187–209.

[16] J. H. E. Cartwright, *Nonlinear stiffness, Lyapunov exponents, and attractor dimension*, Physics Letters A, 1999, 264(4), 298–302.

[17] W. S. Chung, *Fractional Newton mechanics with conformable fractional derivative*, Journal of Computational and Applied Mathematics, 2015, 290, 150–158.

[18] Y. Cui, H. He, G. Sun and C. Lu, *Analysis and control of fractional order generalized Lorenz chaotic system by using finite time synchronization*, Adv. Math. Phys., 2019, 1–12. DOI: 10.1155/2019/3713789.

[19] O. Edward, G. Celso and A. Y. James, *Controlling chaos*, Physical Review Letters, 1990, 64(11), 1196–1199.

[20] E. M. Elabbasy, A. A. Elsadany and Y. Zhang, *Bifurcation analysis and chaos in a discrete reduced Lorenz system*, Applied Mathematics and Computation, 2014, 228, 184–194.

[21] A. A. Elsadany and A. E. Matouk, *Dynamical behaviors of fractional-order Lotka–Volterra predator–prey model and its discretization*, Journal of Applied Mathematics and Computing, 2015, 49(1), 269–283.

[22] A. Elsonbaty and A. A. Elsadany, *Bifurcation analysis of chaotic geomagnetic field model*, Chaos, Solitons & Fractals, 2017, 103, 325–335.

[23] Z. Eskandari, P. A. Naik and M. Yavuz, *Dynamical behaviors of a discrete-time prey–predator model with harvesting effect on the predator*, J. Appl. Anal. Comput, 2024, 14, 283–297.

[24] C. E. Frouzakis, I. G. Kevrekidis and B. B. Peckham, *A route to computational chaos revisited: Noninvertibility and the breakup of an invariant circle*, Physica D: Nonlinear Phenomena, 2003, 177(1–4), 101–121.

[25] Y. Gao annd B. Liu, *Study on the dynamical behaviors of a two-dimensional discrete system*, Nonlinear Analysis: Theory, Methods & Applications, 2009, 70(12), 4209–4216.

[26] Y. Gu, G. Li, X. Xu, X. Song and H. Zhong, *Solution of a new high-performance fractional-order Lorenz system and its dynamics analysis*, Nonlinear Dynamics, 2023, 111(8), 7469–7493.

[27] Z. Hu, Z. Teng and L. Zhang, *Stability and bifurcation analysis of a discrete predator–prey model with nonmonotonic functional response*, Nonlinear Analysis: Real World Applications, 2011, 12(4), 2356–2377.

[28] C. Huang, J. Cao, M. Xiao, A. Alsaedi and F. E. Alsaadi, *Controlling bifurcation in a delayed fractional predator–prey system with incommensurate orders*, Applied Mathematics and Computation, 2017, 293, 293–310.

[29] C. Huang, J. Cao, M. Xiao, A. Alsaedi and T. Hayat, *Bifurcations in a delayed fractional complex-valued neural network*, Applied Mathematics and Computation, 2017, 292, 210–227.

[30] C. Huang, J. Cao, M. Xiao, A. Alsaedi and T. Hayat, *Effects of time delays on stability and Hopf bifurcation in a fractional ring-structured network with arbitrary neurons*, Communications in Nonlinear Science and Numerical Simulation, 2018, 57, 1–13.

[31] C. Huang, Y. Meng, J. Cao, A. Alsaedi and F. E. Alsaadi, *New bifurcation results for fractional BAM neural network with leakage delay*, Chaos, Solitons & Fractals, 2017, 100, 31–44.

[32] M. Ichise, Y. Nagayanagi and T. Kojima, *An analog simulation of non-integer order transfer functions for analysis of electrode processes*, Journal of Electroanalytical Chemistry and Interfacial Electrochemistry, 1971, 33(2), 253–265.

[33] H. Jafari and V. Daftardar-Gejji, *Solving a system of nonlinear fractional differential equations using Adomian decomposition*, Journal of Computational and Applied Mathematics, 2006, 196(2), 644–651.

[34] A. Jajarmi and D. Baleanu, *A new iterative method for the numerical solution of high-order non-linear fractional boundary value problems*, Frontiers in Physics, 2020, 8, 220.

[35] Z. Jing and J. Yang, *Bifurcation and chaos in discrete-time predator–prey system*, Chaos, Solitons & Fractals, 2006, 27(1), 259–277.

[36] S. Kartal and F. Gurcan, *Discretization of conformable fractional differential equations by a piecewise constant approximation*, International Journal of Computer Mathematics, 2019, 96(6), 1849–1860.

[37] R. Khalil, M. A. Horani, A. Yousef and M. Sababheh, *A new definition of fractional derivative*, J. Comput. Appl. Math., 2014, 264, 65–70. DOI: 10.1016/j.cam.2014.01.

[38] A. Q. Khan, S. A. H. Bukhari and M. B. Almatrafi, *Global dynamics, Neimark-Sacker bifurcation and hybrid control in a Leslie's prey-predator model*, Alexandria Engineering Journal, 2022, 61(12), 11391–11404.

[39] A. Q. Khan and T. Khalique, *Neimark-Sacker bifurcation and hybrid control in a discrete-time Lotka-Volterra model*, Mathematical Methods in the Applied Sciences, 2020, 43(9), 5887–5904.

[40] E. N. Lorenz, *Computational chaos-a prelude to computational instability*, Physica D: Nonlinear Phenomena, 1989, 35(3), 299–317.

[41] C. Luo and X. Wang, *Chaos in the fractional-order complex Lorenz system and its synchronization*, Nonlinear Dynamics, 2013, 71, 241–257.

[42] S. Lynch and others, *Dynamical Systems with Applications using Mathematica*, Springer, 2007.

[43] S. Momani and Z. Odibat, *Numerical approach to differential equations of fractional order*, Journal of Computational and Applied Mathematics, 2007, 207(1), 96–110.

[44] D. Mozyrska and W. Małgorzata, *Stability analysis of discrete-time fractional-order Caputo-type Lorenz system*, 42nd International Conference on Telecommunications and Signal Processing (TSP), IEEE, 2019, 149–153. DOI: 10.1109/TSP.2019.8768861.

[45] P. A. Naik, Z. Eskandari, H. E. Shahkari and K. M. Owolabi, *Bifurcation analysis of a discrete-time prey-predator model*, Bulletin of Biomathematics, 2023, 1(2), 111–123.

[46] P. A. Naik, Z. Eskandari, M. Yavuz and J. Zu, *Complex dynamics of a discrete-time Bazykin–Berezovskaya prey-predator model with a strong Allee effect*, Journal of Computational and Applied Mathematics, 2022, 413, 114401.

[47] C. M. A. Pinto and J. T. Machado, *Fractional model for malaria transmission under control strategies*, Computers & Mathematics with Applications, 2013, 66(5), 908–916.

[48] I. Podlubny, *Fractional Differential Equations*, NewYork: Academic Press, 1999.

[49] Z. F. El Raheem and S. M. Salman, *On a discretization process of fractional-order logistic differential equation*, Journal of the Egyptian Mathematical Society, 2014, 22(3), 407–412.

[50] S. M. Rana, *Dynamics and chaos control in a discrete-time ratio-dependent Holling-Tanner model*, Journal of the Egyptian Mathematical Society, 2019, 27(1), 1–16.

[51] S. M. Rana and U. Kulsum, *Bifurcation analysis and chaos control in a discrete-time predator-prey system of Leslie type with simplified Holling type IV functional response*, Discrete Dynamics in Nature and Society, 2017, 2017. DOI: 10.1155/2017/9705985.

[52] S. M. S. Rana and M. J. Uddin, *Dynamics of a discrete-time chaotic Lü system*, Pan-American Journal of Mathematics, 2022, 1, 7. DOI: 10.28919/cpr-pajm/1-7.

[53] M. Richard, D. Manuel, P. Igor and T. Juan, *On the fractional signals and systems*, Signal Processing, 2011, 91(3), 350–371.

[54] S. M. Salman, A. M. Yousef and A. A. Elsadany, *Stability, bifurcation analysis and chaos control of a discrete predator-prey system with square root functional response*, Chaos, Solitons & Fractals, 2016, 93, 20–31.

[55] C. Sparrow, *The Lorenz Equations*, Springer, New York, 1982, 269.

[56] N. Tahir, R. Ahmed and N. A. Shah, *Complex dynamics of a discrete-time Leslie–Gower predator–prey system with herd behavior and slow–fast effect on predator population*, International Journal of Biomathematics, 2024, 2450040, 26.

[57] M. J. Uddin, M. B. Almatrafi and S. Monira, *A study on qualitative analysis of a discrete fractional order prey-predator model with intraspecific competition*, Commun. Math. Biol. Neurosci., 2024, 2024. DOI: 10.28919/cmbn/8477.

[58] M. J. Uddin and S. M. S. Rana, *Analysis of chaotic dynamics: A fractional order glycolysis model*, Network Biology, 2022. http://www.iaees.org/publications/journals/nb/articles/2022-12(4)/2022-12(4).asp.

[59] M. J. Uddin and S. M. Sohel Rana, *Qualitative analysis of the discretization of a continuous fractional order prey-predator model with the effects of harvesting and immigration in the population*, Complexity, 2024, 2024(1). DOI: 10.1155/2024/8855142.

[60] M. J. Uddin, S. M. S. Rana, S. Işık and F. Kangalgil, *On the qualitative study of a discrete fractional order prey–predator model with the effects of harvesting on predator population*, Chaos, Solitons & Fractals, 2023, 175, 113932.

[61] X. Xie, L. Zujun and W. Hui, *An image information hiding algorithm based on chaotic permutation*, NJ Inf. Secur. Commun., 2007, 6, 187–191.

[62] Y. Xie, *A fractional-order discrete Lorenz map*, Advances in Mathematical Physics, 2022, 1, 2881207.

[63] Y. Xu, R. Gu, H. Zhang and D. Li, *Chaos in diffusionless Lorenz system with a fractional order and its control*, International Journal of Bifurcation and Chaos, 2012, 22(04), 1250088.

[64] L. G. Yuan and Q. G. Yang, *Bifurcation, invariant curve and hybrid control in a discrete-time predator–prey system*, Applied Mathematical Modelling, 2015, 39(8), 2345–2362.